ISSN 2039-7941
Anno 2016_Numero 345

rapporti tecnici INGV

Towards the Mediterranean Forecasting System MyOcean V5: numerical experiments results and validation

345

Istituto Nazionale di Geofisica e Vulcanologia

Segreteria di Redazione
Francesca Di Stefano - Referente
Rossella Celi
Tel. +39 06 51860068
redazionecen@ingv.it

in collaborazione con:
Barbara Angioni (RM1)

REGISTRAZIONE AL TRIBUNALE DI ROMA N.173 | 2014, 23 LUGLIO

Rappresentante legale: Carlo DOGLIONI
Sede: Via di Vigna Murata, 605 | Roma

ISSN 2039-7941
Anno 2016_Numero 345

rapporti tecnici INGV

TOWARDS THE MEDITERRANEAN FORECASTING SYSTEM MYOCEAN V5: NUMERICAL EXPERIMENTS RESULTS AND VALIDATION

Damiano Delrosso[1], Emanuela Clementi[1], Alessandro Grandi[1], Marina Tonani[1,*], Paolo Oddo[1,**], Giacomo Girardi Feruzza[1,***], Nadia Pinardi[1,2,3]

[1]**INGV** (Istituto Nazionale di Geofisica e Vulcanologia, Sezione di Bologna)
[2]**CMCC** (Centro Euro-Mediterraneo sui Cambiamenti Climatici, Bologna)
[3]**UNIVERSITÀ DEGLI STUDI DI BOLOGNA** (Dipartimento di Fisica e Astronomia)

[*]now at: Met Office, Exeter, UK
[**]now at: NATO Science and Technology Organization Centre for Maritime Research and Experimentation, La Spezia
[***]now at: F.lli Scuttari S.a.s., Chioggia

345

Table of Contents

Introduction 7

1. MFS MyOcean V4 description 9

1.1 NEMO component 9

1.2 Data assimilation component 9

1.3 WWIII component 10

1.4 NEMO – WWIII coupling 10

2. Evolution of MFS from MyOcean V4 to MyOcean V5 11

2.1 Formulation of the bottom drag coefficient according to the law of the wall 11

2.2 MFS Nesting into the daily real time Mercator Ocean Global Ocean Forecasting System 11

2.3 Horizontal eddy diffusivity for tracers and horizontal eddy viscosity 13

2.4 Tracer advection 13

2.5 Momentum advection 14

3. Experiments description 14

4. Experiments results and validation 16

4.1 Basin averaged time series (Temperature, Salinity, Currents, Sea Surface Height) 16

4.2 Misfits (Temperature, Salinity, Sea Level Anomaly) 20

4.3 CalVal buoys (Temperature, Salinity, Currents, Sea Surface Height) 24

4.4 Estimated Accuracy Numbers (Temperature, Salinity, Sea Surface Temperature, Sea Level Anomaly) 29

4.5 ARGO Profiles 35

4.6 GLIDER Profiles (Temperature and Salinity) in the Balearic Sea 39

4.7 T/S Diagrams in the Balearic Sea area 45

4.8 Waves: basin averaged time series and CalVal buoys 48

5. Conclusions 50

References 50

Introduction

This work describes a set of numerical experiments carried out using a coupled wave-ocean modeling system implemented in the Mediterranean Sea in order to meet the needs of an improvement of the operational sea state and current analysis and forecasts in the framework of the MyOcean FollowOn project.

MyOcean is a series of projects granted by the European Commission within the GMES Program (Seventh Framework Program), whose objective is a pan-European capacity for ocean monitoring and forecasting.

INGV is responsible for the production of two products within MyOcean:

- Mediterranean Sea Physics Analysis and Forecast (MEDSEA_ANALYSIS_FORECAST_PHYS_006_001_a).
- Mediterranean Sea Physics Reanalysis (MEDSEA_REANALYSIS_PHYS_006_004).

In particular, the main focus of the present work has been to investigate a series of hydrodynamic model developments to provide enhanced analysis and forecast products.

The physical component of the Mediterranean Forecasting System (MFS) for analysis and forecast is a coupled hydrodynamic-wave model implemented over the whole Mediterranean Basin. The model horizontal grid resolution is 1/16˚ (6-7 km, approximately) and is resolved over 72 unevenly spaced z-vertical levels.

The hydrodynamics are supplied by the Nucleus for European Modelling of the Ocean (NEMO) while the wave component is provided by WaveWatch-III (hereafter denoted as WWIII). The model solutions are corrected by the variational assimilation (based on a 3D-VAR scheme) of temperature and salinity vertical profiles and along track satellite sea level anomaly observations.

The analysis is done weekly, on Tuesday, for the previous 15 days. The assimilation cycle is daily (24hr) and is done in filter mode. 10-day forecast is produced every day. The forecast is initialized by a hindcast every day except Tuesday, when the analysis is used instead of the hindcast.

The temporal evolution of the Mediterranean Forecasting System in the framework of MyOcean projects series is summarized in Table 1.

MYOCEAN VERSION	OPERATIONAL SINCE	SYSTEM NAME, NEMO MODEL VERSION AND INITIAL CONDITIONS	MAIN FEATURES INTRODUCED	PRODUCTS
V0	2009 Sep	**SYS4a2** NEMO 3.1	- Lateral Open Boundary Conditions from Global System (monthly mean climatology based on 3 years run)	Potential Temperature, Salinity, Zonal and Meridional Velocity, Sea Surface Height
V1	2010 Dec	**SYS4a3** NEMO 3.1(1997-2010) Initial Conditions from **SDN-V3** **SYS4b** NEMO 3.1 NEMO-WAM		Potential Temperature, Salinity, Zonal and Meridional Velocity, Sea Surface Height
V2	2012 Jan	**SYS4a4** NEMO 3.1 (1997-2011) Initial Conditions from **SDN-V3** **SYS4b2** NEMO 3.1 NEMO-WAM	- Lateral Open Boundary Conditions from Global System (monthly mean clim based on 10 years run) - True stress - Wind drag coefficient	Potential Temperature, Salinity, Zonal and Meridional Velocity, Sea Surface Height Zonal and Meridional Stokes drift velocity Wave number

V3	2013 Apr	**SYS4a5** NEMO 3.4 (2009-2012) Initial Conditions from **SYS4a4** (comparison SYS4a4-SYS4a5) **SYS4c** NEMO 3.4 NEMO-WW-III (Initial Conditions from SYS4b2)	- Porting to new machine	Potential Temperature, Salinity, Zonal and Meridional Velocity, Sea Surface Height Zonal and Meridional Stokes drift velocity Wave number
V4	2014 Apr	**SYS4d** NEMO 3.4 (25/12/2012-2014) NEMO-WW-III Initial Conditions from SYS4a5	- Atmospheric Pressure - Time Splitting - TAPAS assimilation	Potential Temperature, Salinity, Zonal and Meridional Velocity, Sea Surface Height Stokes drift Wave number
V5	2015 Mar	**SYS4e** NEMO 3.4 (2011-ongoing) NEMO-WW-III Initial Conditions from SDN-V3	- Formulation of the bottom drag coefficient according to the law of the wall - Nesting of the Mediterranean Forecasting System into the daily real time Mercator Ocean Global Ocean Forecasting System - Modified horizontal eddy diffusivity for tracers and horizontal eddy viscosity - New glider assimilation - Time step reduction	Potential Temperature, Salinity, Zonal and Meridional Velocity, Sea Surface Height Zonal and Meridional Stokes drift velocity Wave number

Table 1. Temporal evolution of the Mediterranean Forecasting System in the framework of MyOcean projects series.

This work deals with the numerical experiments carried out during the testing phase which led to the implementation of the new Mediterranean Forecasting System (MFS) for MyOcean V5, named hereafter sys4e, starting from the Mediterranean Forecasting System for MyOcean V4, named hereafter sys4d.

In order to quantify the impact of the modifications introduced into the NEMO model set-up, each numerical experiment has been validated by using:

- buoys data for temperature, salinity, currents, sea surface height, significant wave height, mean wave period and peak wave period;
- ARGO floats and gliders data for temperature and salinity;
- satellite data for sea level anomaly and sea surface temperature.

Moreover, basin averaged time series of the above mentioned variables have been computed in order to compare each experiment with the reference system (sys4d).

This report is organized as follows: section 1 describes the MFS System for MyOcean V4 and its numerical components; section 2 highlights the main model evolution from MyOcean V4 to MyOcean V5, section 3 illustrates the numerical tests that have been performed in order to reach the final MyOcean V5 configuration, in section 4 all the numerical results and their validation against in situ and remote sensing measurements are presented and conclusions are summarized in section 5.

1. MFS MyOcean V4 description

The oceanic equations of motion of the Med-currents system are solved by two elements: an Ocean General Circulation Model (OGCM) and a Wave Model. The OGCM code is based on NEMO version 3.4 [Madec et al., 2008]. The code is developed and maintained by the NEMO-consortium. The wave dynamics is solved by a Mediterranean implementation of the WWIII code version 3.14 [Tolman, 2009].

NEMO and WWIII models are two-way coupled every hour.

1.1 NEMO component

NEMO model has been implemented in the Mediterranean Sea at 1/16° x 1/16° horizontal resolution and 72 unevenly spaced z-vertical levels with partial cells [Oddo et al., 2009]. Figure 1 shows the bathymetry and the model domain: Mediterranean Sea extended into the Atlantic Ocean to which it is connected through the Strait of Gibraltar that provides a major inflow of water.

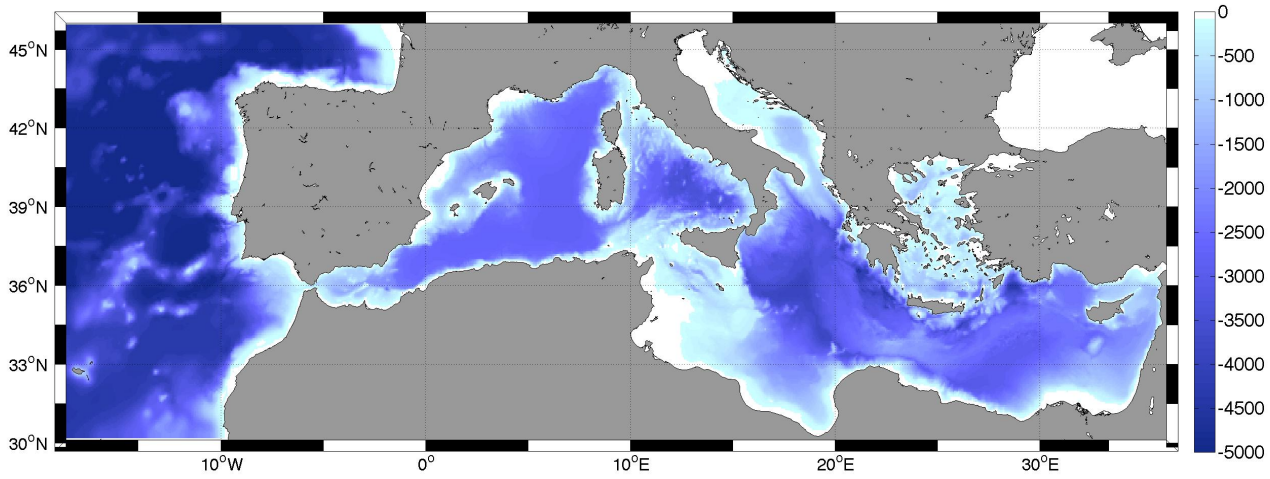

Figure 1. Representation of the model domain and bathymetry: Mediterranean Sea extended into the Atlantic.

The NEMO code solves the primitive equations using the time-splitting technique that is the external gravity waves are explicitly resolved. Also the atmospheric pressure effect has been introduced in the model dynamic [Oddo et al., 2014]. The code is run with linear free surface formulation and fixed volume.

The hydrodynamic model of the MFS for MyOcean is nested, in the Atlantic, within the monthly mean climatological fields computed from ten years of daily output of the 1/4° x 1/4° degrees global model [Drevillon et al., 2008]. Details on the nesting technique and major impacts on the model results are in Oddo et al., 2009. The model uses vertical partial cells to fit the bottom depth shape.

The model is forced by momentum, water and heat fluxes interactively computed by bulk formulae using the 6-h, 0.25° horizontal-resolution operational analysis and forecast fields from the European Centre for Medium-Range Weather Forecasts (ECMWF) and the model predicted surface temperatures (details of the air-sea physics are in Tonani et al. [2008]). The water balance is computed as Evaporation minus Precipitation and Runoff. The evaporation is derived from the latent heat flux while the precipitation and the runoff are provided by monthly mean datasets: the Climate Prediction Centre Merged Analysis of Precipitation (CMAP) Data [Xie and Arkin, 1997]; the Global Runoff Data Centre dataset [Fekete et al., 1999] for Po, Ebro, Nile and Rhone, the dataset from Raicich [1996] for the Adriatic rivers Vjosë, Seman, and Buna-Bojana.

The Dardanelles inflow is parameterized as a river and the climatological net inflow rates are taken from Kourafalou and Barbopoulos [2003].

1.2 Data assimilation component

The data assimilation system is the OCEANVAR scheme developed by Dobricic and Pinardi [2008]. The background error correlation matrix is estimated from the temporal variability of parameters in a

historical model simulation. Background error correlation matrices vary seasonally and in 13 regions of the Mediterranean Sea, which have different physical characteristics [Dobricic et al., 2007]. The mean dynamic topography used for the assimilation of SLA (Sea Level Anomaly) has been computed by Dobricic et al. [2005]. The assimilated data include: sea level anomaly, sea surface temperature, in situ temperature profiles by VOS XBTs (Voluntary Observing Ship-eXpandable Bathythermograph), in situ temperature and salinity profiles by argo floats, and in situ temperature and salinity profiles from CTD (Conductivity-Temperature-Depth). For what concerns SLA data a dedicated satellite product accounting for atmospheric pressure effect is used. Satellite OA-SST (Objective Analyses-Sea Surface Temperature) data are used for the correction of surface heat fluxes with the relaxation constant of 40 W m-2 K-1.

1.3 WWIII component

The wave model solves the wave action balance equation that describes the evolution, in slowly varying depth domain and currents, of a 2D ocean wave spectrum where individual spectral component satisfies locally the linear wave theory. In the present application WWIII has been implemented following WAM cycle4 model physics [Gunther et al., 1993]. Wind input and dissipation terms are based on Janssen's quasi-linear theory of wind-wave generation [Janssen, 1989, 1991]. The dissipation term is based on Hasselmann [1974] whitecapping theory according to Komen et al. [1984]. The non-linear wave-wave interaction is modelled using the Discrete Interaction Approximation [DIA, Hasselmann et al., 1985]. No interactions with the ocean bottom are considered.

The implementation of WWIII in the Mediterranean Sea follows the same horizontal resolution of NEMO while the spectral discretization is achieved through 30 frequency bins ranging from 0.05 to 0.79 Hz and 24 equally distributed directional bins.

The wave model has been forced by the same ¼ degree horizontal resolution ECMWF atmospheric forcings used to force the hydrodynamic model. The wind speed is then modified by considering a stability parameter depending on the air-sea temperature difference according to Tolman [2002].

1.4 NEMO – WWIII coupling

The NEMO model provides hourly estimates of air-sea surface temperature difference and surface currents to WWIII which returns back to NEMO the neutral component of the surface drag coefficient taking into account wave induced effect at the air-sea interface. Model coupling is presented in Figure 2 and described in Clementi et al. [2013].

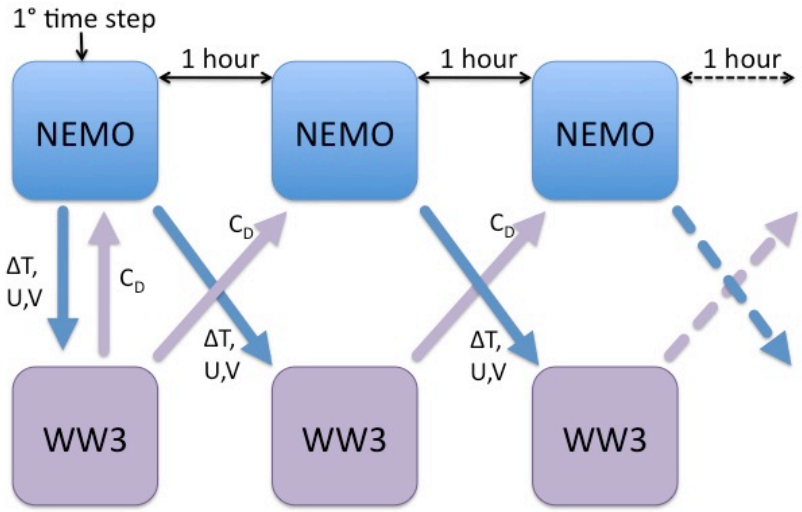

Figure 2. Sketch of the coupling mechanism between WWIII and NEMO. When the simulation starts, models exchange information after the first time step (10 min), while later they communicate every hour. NEMO sends to WWIII air-sea temperature difference (ΔT) and current fields (U,V), while WWIII passes to NEMO the neutral drag coefficient (CD).

2. Evolution of MFS from MyOcean V4 to MyOcean V5

In order to meet the requirements of the European Commission MyOcean2 and MyOcean Follow-on projects, several numerical experiments have been carried out, aiming at implementing and testing new features and developments with respect to the MFS MyOcean V4 (sys4d) and achieving the final MyOcean V5 (sys4e) configuration. The set of tested modifications are briefly described in the following sections from 2.1 to 2.3.

2.1 Formulation of the bottom drag coefficient according to the law of the wall

The hydrodynamic model bottom boundary condition is based on a quadratic form of the bottom friction with split-explicit time splitting. NEMO version 3.4 provides a bottom drag coefficient that is not scaled with respect to the lowermost bottom cell thickness causing relevant issue in case of z-coordinate partial steps interpolation (used in the MFS MyOcean V4 model implementation) and not satisfying the law of the wall.

The formulation of the bottom drag coefficient has then been updated with respect to sys4d following a logarithmic formulation calculated as:

$$Cd = \max\left[Cd_{\min'} \left\{ k^{-1} \ln\left(\frac{dz_b}{2z_{0b}} \right) \right\}^{-2} \right] \quad (1)$$

where k=0.4 is the Von Karman constant, $Cd_{\min}$=1.e-5 is the minimum drag coefficient, dz_b is the lowermost bottom cell thickness and $z0_b$=1.e-2 is the bottom roughness.

2.2 MFS Nesting into the daily real time Mercator Ocean Global Ocean Forecasting System

An important model improvement considered the nesting of the Atlantic part of the MFS domain within daily real time analyses and forecasts from Mercator Ocean - Global Ocean Forecasting System (GLO-MFC). The sys4d used instead climatological monthly mean values of velocities and tracers as described in Oddo et al. [2009].

For the nested boundary conditions considered:

1) The radiative phase velocity (C_x and C_y) is computed at the open boundaries [Marchesiello et al., 2001];
2) The radiation algorithm is applied to zonal and meridional components of the open boundary conditions velocities using the phase velocities computed at point 1;
3) The Flather boundary condition [Flather, 1976] is applied to barotropic velocities at open boundaries for the time-splitting free surface case;
4) The total velocities are updated on the basis of point 2 and 3;
5) For tracers the 2D radiation condition is applied using radiative phase velocity computed at point 1.

Two daily lateral open boundary condition (LOBC) datasets have been considered from the GLO-MFC: the first covers the period from January 2007 to December 2012 and derives from a pre-operational global model implementation; the second covers the period January 2013 – May 2014 and has been retrieved from global products of the MyOcean catalogue.

The daily products of the first dataset are provided on native Mercator Ocean curvilinear grid, while the second daily operational dataset are provided on a regular grid according to the MyOcean operational procedure.

For each dataset a twin experiment has been performed in order to evaluate the impact of daily lateral boundary conditions with respect to monthly climatology lateral boundary conditions.

The two GLO-MFC daily data sets (1/12° horizontal resolution, 50 vertical levels) have been interpolated onto the MFS grid (1/16° horizontal resolution, 72 vertical levels). An example is shown in Figure 3.

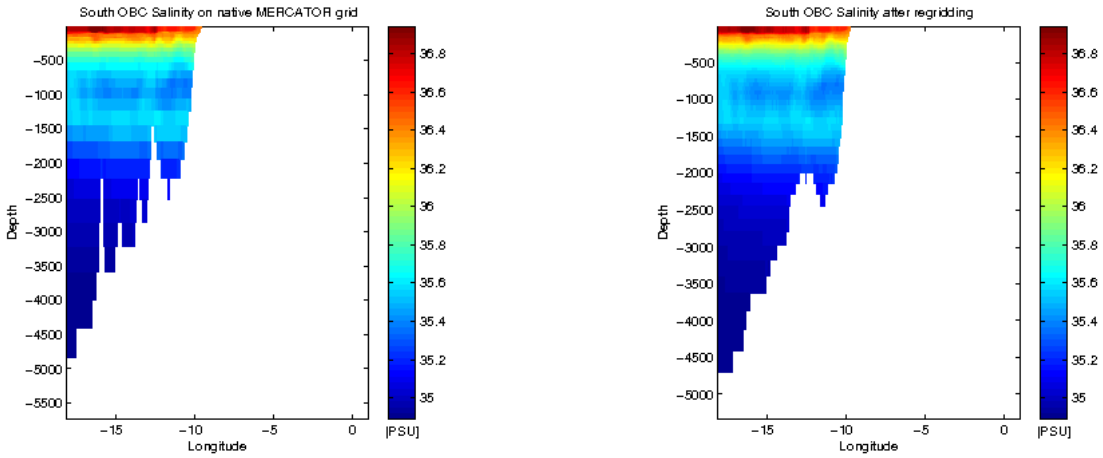

Figure 3. Example of interpolation from Mercator Ocean grid to MFS grid.

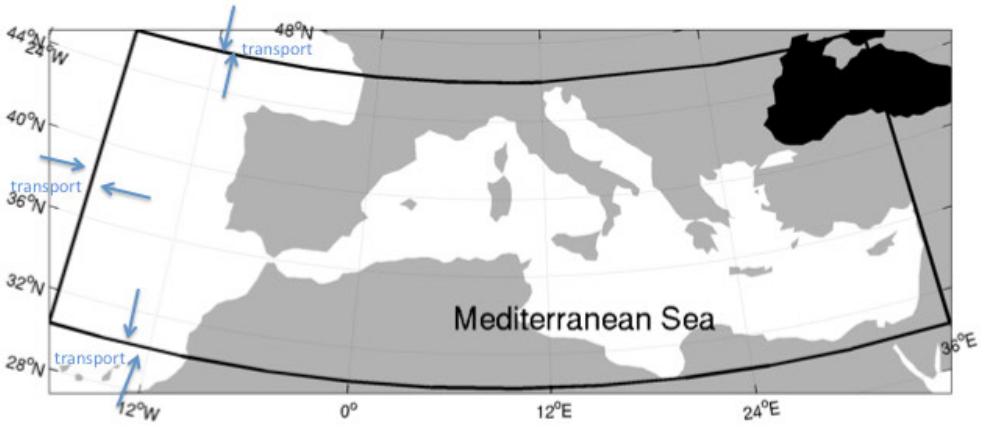

Figure 4. Model domain showing open boundaries at the western side of the basin and representation of the transport.

A transport constraint [Pinardi et al., 2003] has been applied to each boundary (Figure 4 and 5), in order to conserve the transport through the boundaries after the interpolation of velocity components from native grid to destination grid.

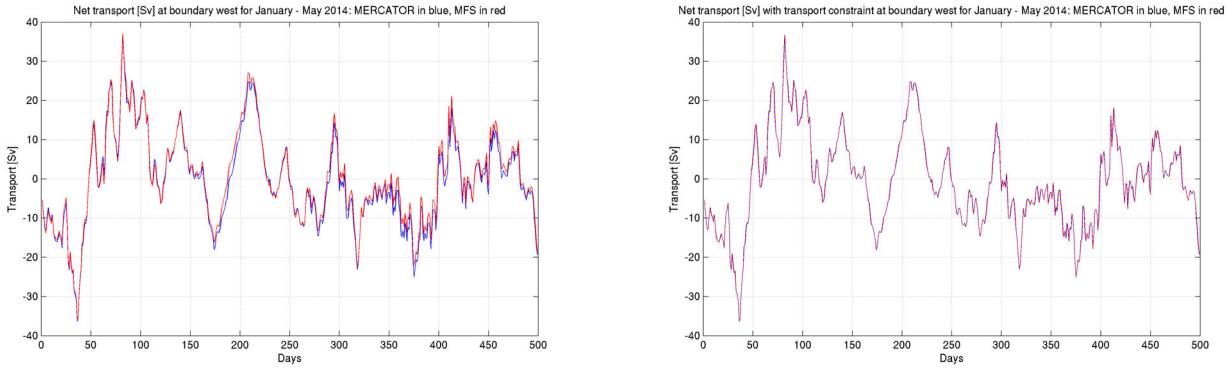

Figure 5. Example of transport constraint applied to velocity normal component after the interpolation from Mercator Ocean grid to MFS grid.

The two daily lateral open boundary conditions datasets derived from GLO-MFC have been used to force the numerical experiments performed to reach the setup of the MFS sys4e.

In order to ensure more numerical stability the time step of the numerical simulations performed has been reduced from 600s, used in the MFS sys4d, to 300s.

2.3 Horizontal eddy diffusivity for tracers and horizontal eddy viscosity

For the lateral diffusion of tracers a bilaplacian operator is used, which consists in applying twice the laplacian of tracers (already multiplied by the eddy diffusivity coefficient *A*), described in the following equation:

$$D_T^{lT} = \frac{1}{b_t T}\left(\delta_i \left[A_u^{lT} \, \frac{e_{2u}\, e_{3u}}{e_{1u}} \, \delta_{i+1/2}[T] \right] + \delta_j \left[A_v^{lT} \, \frac{e_{1v}\, e_{3v}}{e_{2v}} \, \delta_{j+1/2}[T] \right] \right) \tag{2}$$

In the above equation *T* is the tracer, A_u^{lT} is the horizontal diffusivity coefficient in *u* (zonal velocity) direction, A_v^{lT} is the horizontal diffusivity coefficient in *v* (meridional velocity) direction, $b_t = e_{1t} e_{2t} e_{3t}$ is the volume of T–cells, e_{1u},e_{2u},e_{3u} are the dimensions of U-cells, e_{1v},e_{2v},e_{3v} are the dimensions of V-cells.

For the lateral diffusion of momentum a bilaplacian operator is used, which separates the divergent and rotational parts of the flow: it consists in applying a second time the laplacian operator described in the following equation, after having multiplied it by the eddy viscosity coefficient:

$$\begin{cases} D_u^{l\mathbf{U}} = \dfrac{1}{e_{1u}} \delta_{i+1/2} \left[A_T^{lm} \, \chi \right] - \dfrac{1}{e_{2u}\, e_{3u}} \delta_j \left[A_f^{lm} \, e_{3f} \zeta \right] \\ \\ D_v^{l\mathbf{U}} = \dfrac{1}{e_{2v}} \delta_{j+1/2} \left[A_T^{lm} \, \chi \right] + \dfrac{1}{e_{1v}\, e_{3v}} \delta_i \left[A_f^{lm} \, e_{3f} \zeta \right] \end{cases} \tag{3}$$

In the above equation $A_T^{lm} \chi$ is the horizontal divergence, $A_f^{lm} e_{3f} \zeta$ is the relative vorticity.

In the numerical experiments performed to reach the set up of MFS sys4e the eddy horizontal diffusivity coefficient and the eddy horizontal viscosity coefficient have been modified and several parametrizations have been tested, in order to evaluate also a different setting of the Prandtl number, given by viscosity coefficient/diffusivity coefficient, as shown in Table 4.

2.4 Tracer advection

The advection tendency of a tracer in flux form is the divergence of the advective fluxes. Its discrete expression is given by:

$$ADV_\tau = -\frac{1}{b_t} \left(\delta_i \left[e_{2u}\, e_{3u}\, u\, \tau_u \right] + \delta_j \left[e_{1v}\, e_{3v}\, v\, \tau_v \right] \right) - \frac{1}{e_{3t}} \, \delta_k \left[w\, \tau_w \right] \tag{4}$$

where τ_u,τ_v and τ_w are either temperature or salinity along *u*, *v* and w velocity components.

The tracer advection schemes tested are a Monotone Upstream Scheme for Conservative Laws (MUSCL) and a Total Variance Dissipation Scheme (TVD).

In the formulation of MUSCL scheme, the tracer at velocity points is evaluated assuming a linear tracer variation between two T–points.

In the TVD formulation, the tracer at velocity points is evaluated using a combination of an upstream and a centered scheme: in the latter the tracer at velocity points is evaluated as the mean of the two neighbouring T-point values.

2.5 Momentum advection

Two different formulations of the momentum advection have been tested in the experiments performed: the vector invariant form and the flux form of the momentum advection term.

The vector formulation is given by:

$$\left[(\nabla \times \mathbf{U}) \times \mathbf{U} + \frac{1}{2}\nabla\left(\mathbf{U}^2\right)\right]_h = \zeta\, \mathbf{k} \times \mathbf{U}_h + \frac{1}{2}\nabla_h\left(\mathbf{U}_h^2\right) + \frac{1}{e_3} w \frac{\partial \mathbf{U}_h}{\partial k} \tag{5}$$

where ζ is the vorticity, k is the local upward vector, U is the vector velocity, w is the vertical velocity component and e_3 is the vertical dimensions of the cells.

The flux form formulation is given by:

$$\left[(\nabla \times \mathbf{U}) \times \mathbf{U} + \frac{1}{2}\nabla\left(\mathbf{U}^2\right)\right]_h = \nabla \cdot \begin{pmatrix} \mathbf{U}\, u \\ \mathbf{U}\, v \end{pmatrix} + \frac{1}{e_1 e_2}\left(v\frac{\partial e_2}{\partial i} - u\frac{\partial e_1}{\partial j}\right)\mathbf{k} \times \mathbf{U}_h \tag{6}$$

The first term of the right-hand side of the above equation is the divergence of momentum fluxes, while the second term is the so-called metric term, which is a modification of the Coriolis parameter due to the curvilinear nature of the coordinate system used.

3. Experiments description

The six experiments considered in order to define the MFS sys4e setup and the configuration differences between them (namely: sys4d, V1, V5, V7, V8, V9) are summarized in Table 2.

Experiment	sys4d	V1	V5	V7	V8	V9
Model settings						
Lateral Open Boundary Conditions	Climatological	Daily	Daily	Daily	Daily	Daily
Tracer advection	MUSCL	MUSCL	TVD	MUSCL	MUSCL	MUSCL
Momentum advection	Vector form	Vector form	Flux form (UBS)	Vector form	Vector form	Vector form
Viscosity/Diffusivity [m^4/s]	$-5.e^9$ / $-3.e^9$ (Prandtl=1.67)	$-5.e^9$ / $-3.e^9$ (Prandtl=1.67)	$-1.e^9$ / $-6.e^8$ (Prandtl=1.67)	$-1.e^9$ / $-6.e^8$ (Prandtl=1.67)	$-1.e^9$ / $-2.e^8$ (Prandtl=5)	$-1.e^9$ / $-6.e^8$ (Prandtl=1.67)
Time step	600 sec	300 sec	300 sec	300 sec	300 sec	300 sec
Bottom Drag Coefficient (Cd) scaled with respect to the lowermost bottom cell thickness	no	yes	yes	yes	yes	yes
Initial Conditions	Restart from operational system MED-MFC sys4d (day 20130101)	Restart from operational system MED-MFC sys4d (day 20130101)	Restart from operational system MED-MFC sys4d (day 20130101)	Restart from operational system MED-MFC sys4d (day 20130101)	Restart from operational system MED-MFC sys4d (day 20130101)	SeaDataNet Initial Conditions (day 20130101)

Table 2. Experimental design.

Other experiments have been performed, but only the ones summarized in the above table have been selected and presented in this work in order to define the final setup for MFS sys4e.

The experiment V5 has been performed in order to test the TVD scheme for tracers advection, in combination with flux form for momentum advection.

The goal of the experiment V5 was to test the impact on tracers of an advection scheme, TVD, shown to be less diffusive with respect to MUSCL scheme [Levy et al., 2001].

The experiment V8 has been performed in order to test how an increased viscosity/diffusivity ratio (Prandtl number = 5) affects the vertical mixing processes [Noh, 2004].

The experiment V9 has been performed in order to support the theory that re-initialize the hydrodynamic component of the Mediterranean Forecasting System for MyOcean V5 could have given better results with respect to re-initialize it from a restart file of the previous version of the operational system, namely the one available for MyOcean V4.

All the experiments performed have been tested using:

- daily Lateral Open Boundary Conditions, except the sys4d experiment which is forced by a climatological Lateral Open Boundary Conditions dataset, as discussed in paragraph 2.2;
- linear free surface formulation with fixed volume for surface kinematic equation. The surface kinematic equation is defined as follows [Roullet and Madec, 2000]:

$$\partial_t \eta = u|_{z=\eta} \cdot n + P + R - E \tag{7}$$

where η is the sea surface height relative to the mean sea level; $n = (-\partial_x \eta, -\partial_y \eta, 1)$ is the unit vector normal to the free surface multiplied by the cosine of the free surface angle relative to the horizontal; u is the velocity; *E, P* and *R* are the three components of the fresh water flux (evaporation, precipitation and runoffs).

In the assumption of linear free surface formulation (7) becomes:

$$\partial_t \eta = w|_{z=0} + P + R - E \tag{8}$$

where w is the vertical component of the velocity;

- the MUSCL tracer advection scheme, except experiment V5 which uses the TVD scheme, both discussed in paragraph 2.4;
- the vector form for momentum advection, except experiment V5 which uses the flux form, both discussed in paragraph 2.5;
- different horizontal eddy diffusivity for tracers and horizontal eddy viscosity (whose formulation is explained in paragraph 2.3);
- time step equal to 300 seconds except for the sys4d experiment, where the time step has been set equal to 600 seconds;
- a variable bottom drag coefficient, already discussed in section 2.1 except for sys4d experiment, where a constant bottom drag coefficient has been used;
- a restart file from the MFS sys4d operational production, except the V9 experiment which has been initialized using SeaDataNet initial conditions (the monthly climatologies for temperature used as initial conditions had been calculated with Diva3D, using the semi-normed analysis method, putting as background field the seasonal fields, while for salinity the monthly climatologies had been calculated using the same method, but using the annual mean as background field);
- the assimilation mode (described in section 1.2);
- the coupling with WWIII wave model (described in section 1.4);
- a simulation period that goes from 1st of January 2013 to 30th of September 2014.

The model configuration used for all the performed experiments is summarized in Table 3 and Table 4.

CPP key	Associated process
key_dynspg_ts	Split-explicit free surface
key_mfs	MFS bulk formulation
key_obc	Lateral boundary condition with open boundaries parameters
key_zdfric	Richardson number dependent vertical diffusion
Key_iomput	Outputs are selected in iodef.xml
key_mpp_mpi	Massively Parallel Processing

Table 3. List of the NEMO model configuration CPP (C pre-processor) keys adopted.

	NEMO configuration
Horiz. Resolution	1/16 Degree
Vertical discretization	72 z levels with partial cells (*ln_zps = .true.*)
Air-sea fluxes	MFS-Bulk formulae (*ln_blk_mfs = .true.*)
Neutral drag coefficient	Read from file (*ln_cdgw = .true.*)
Runoff	As Surface boundary condition for S and w (*ln_rnf = .true.*)
Sea Surface Restoring on T and/or S	Yes (*ln_ssr = .true.*)
Solar radiation	2 bands penetration (*ln_qsr_2bd = .true.*)
Lateral momentum B.C.	No-sleep (*rn_shlat = 2*)
Open boundaries	Flather open boundary condition (*ln_obc_fla = .true.*)
Bottom B.C	Non linear friction (*nn_bfr = 2*)
EOS	UNESCO – Jackett and McDougall [1994] (*nn_eos = 0*)
Back. Vertical Visc.	Amv =1.2e-5 m^2 s^{-1}
Back. Vertical Diff.	Avt =1.2e-6 m^2 s^{-1}
Vertical Scheme	Implicit (*ln_zdfexp = .false.*)
Free-surface formulation	Split-explicit (*key_dynspg_ts*)

Table 4. List of the NEMO model configuration setup as defined in namelist.

4. Experiments results and validation

This section presents the numerical experiment results, their intercomparison and their validation according to the available in situ and remote sensing data.

4.1 Basin averaged time series (Temperature, Salinity, Currents, Sea Surface Height)

In this paragraph a comparison between the basin averaged time series of temperature, salinity, currents and sea surface height is shown.

In the left-hand side of Figure 6 the sea surface salinity time series of the performed experiments are shown, while in the right-hand side the differences between the experiments V1, V5, V7, V8 and V9 with respect to sys4d run are shown.

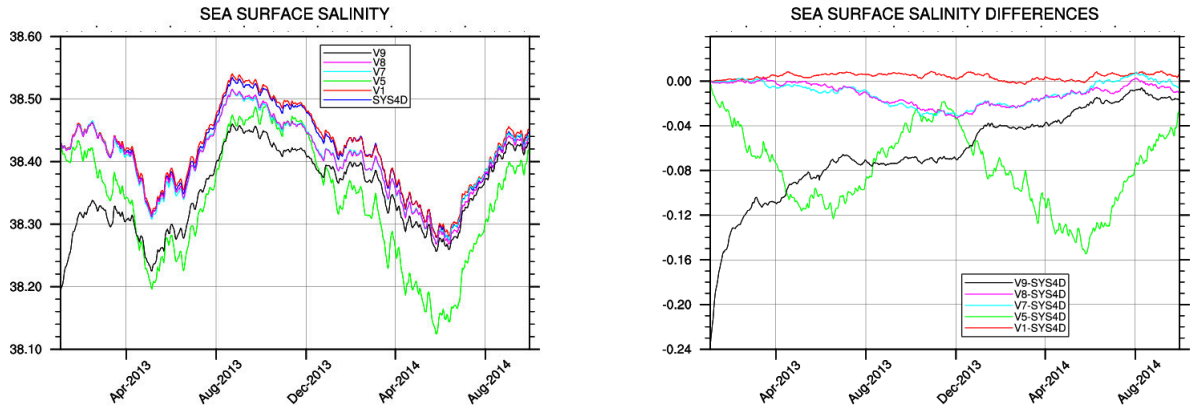

Figure 6. Sea surface salinity [PSU] comparison (left-hand side panel) and differences between the experiments performed and MFS sys4d (right-hand side panel) for the whole period of simulation.

The experiments sys4d, V1, V7 and V8 show a similar behavior from January 2013 to August 2013, when V7 and V8 sea surface salinity starts to decrease respect to sys4d and V1, until June-July 2014, when the curves of the above mentioned experiments starts to converge again. The shape of the curve representing

experiment V5 is very different from all the other experiments performed, due the different momentum and tracers advection schemes used. Major differences can be seen for V9 experiment, started from SeaDataNet initial conditions instead of a restart file of MFS sys4d operational system. It needs about 18 months to converge toward sys4d, V1, V7 and V8 experiments.

In terms of differences between the experiments performed and the operational system MFS sys4d, the right-hand side of Figure 6 shows that V1 experiment has a very similar behavior with respect to sys4d simulation, since the main difference between the setups of the two experiments is only in the implementation of the Lateral Open Boundary Conditions, which are provided daily to V1 experiment, while are provided as climatological mean to sys4d simulation. As already highlighted, V7 and V8 experiments have a very similar behavior and highest differences with respect to sys4d are concentrated from April 2013 to June 2014. V5 experiment shows the largest differences with respect to sys4d due to the big differences in the setup between the two experiments. V9 experiments shows highest differences with respect to the other experiments at the beginning of the simulation that reduces after about 18 months.

The volume mean salinity shows much less differences between the experiments performed with respect to sea surface salinity (Figure 7, left-hand panel).

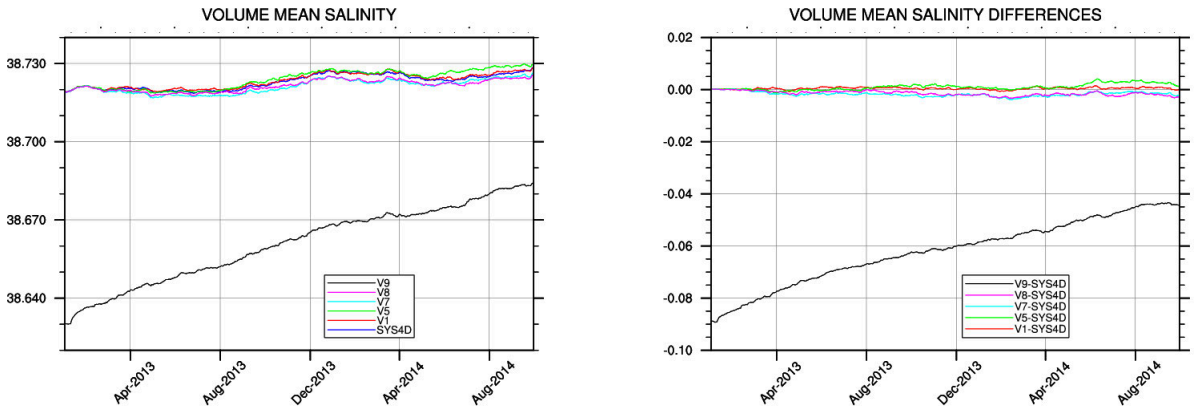

Figure 7. Volume mean salinity [PSU] comparison (left-hand side panel) and differences between the experiments performed and MFS sys4d (right-hand side panel) for the whole period of simulation.

All the experiments show a similar behavior except for V9 experiment that presents a lower volume averaged salinity that increases in time but never reaches values comparable with the other experiments, with a difference of about 0.05 PSU at the end of the simulation.

The volume mean salinity differences of the experiments performed with respect to the MFS sys4d are very little (Figure 7, right-hand panel), in particular for V1 experiment; only the V9 experiment shows a large difference with respect to sys4d, which decreases along the simulation period.

In the left-hand side of Figure 8 the basin averaged sea surface temperature time series are shown, while in the right-hand side the differences between the experiments V1, V5, V7, V8 and V9 with respect to sys4d run are shown.

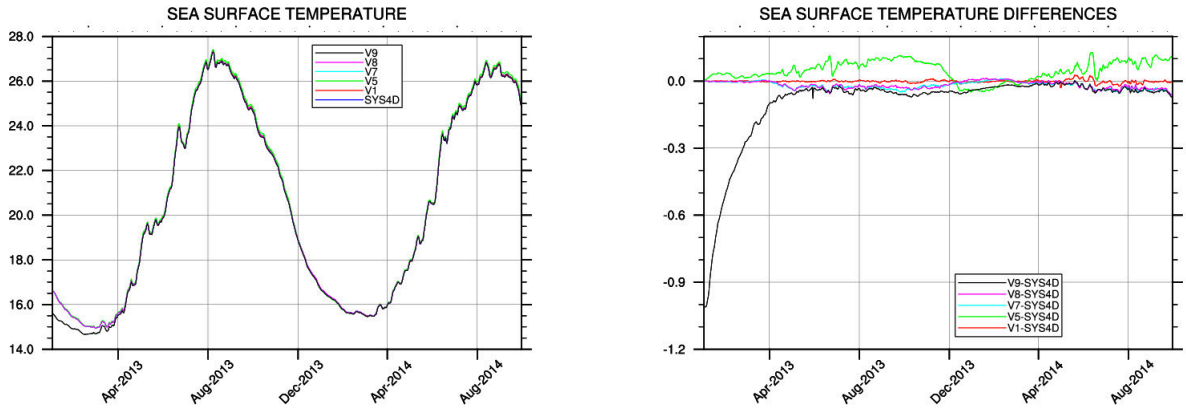

Figure 8. Sea surface temperature [^{o}C] comparison (left-hand side panel) and differences between the experiments performed and MFS sys4d (right-hand side panel) for the whole period of simulation.

The results of all the experiments are very close to each other, except V9 that converges toward the other experiments after 6 months, due to the different initial conditions.

In terms of differences between the simulation performed using the operational system MFS sys4d and the other experiments performed, the right-hand side panel of Figure 7 shows that all the experiments performed are very close to sys4d results, except V9 and V5, the latter showing a sea surface temperature generally higher with respect to all the other experiments performed.

Also the volume mean temperature shows a very similar behavior for all the experiments performed, with the exception of V9, which needs about 18 months to give results comparable with the ones produced by the other experiments (Figure 9, left-hand panel).

In terms of differences between the simulation performed using the operational system MFS sys4d and the other experiments performed, the right-hand side panel of Figure 9 shows that all the experiments performed are very close to sys4d results, in particular V1 experiment, with the exception of V9. In particular V7 and V8 experiments present higher volume mean temperature, and V5 is characterized by a lower temperature with respect to sys4d.

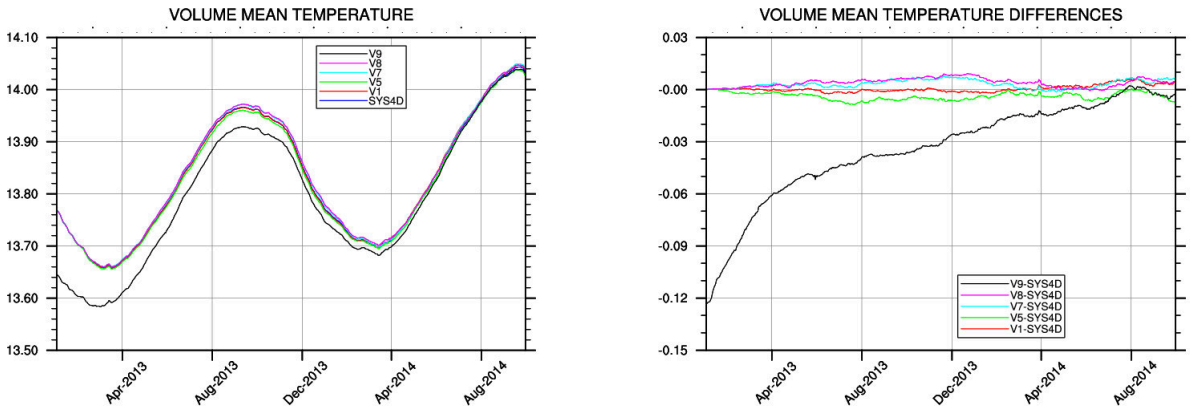

Figure 9. Volume mean temperature [^{o}C] comparison (left-hand side panel) and differences between the experiments performed and MFS sys4d (right-hand side panel) for the whole period of simulation.

The largest differences between the MFS sys4d and the set of experiments performed can be noticed by considering the sea surface height. In Figure 10, left-hand panel, is shown that all the experiments performed have a similar behavior, with the exception of sys4d experiment. It should be noticed that the climatological SSH dataset used as Lateral Open Boundary Conditions for sys4d has been computed using a Mean Sea Surface averaged over a reference period of 5 years (from 2001 to 2005), while the daily SSH dataset used as Lateral Open Boundary Conditions for all the other experiments is an analysis dataset from the Mercator Global Forecasting System, which assimilates SLA data which have a Mean Sea Surface averaged over a 7-years period (from 1993 to 1999).

Looking at the right-hand side of Figure 10, a similar behavior of V1 and V5 with respect to sys4d on the one hand, and V7, V8 and V9 on the other hand can be noticed.

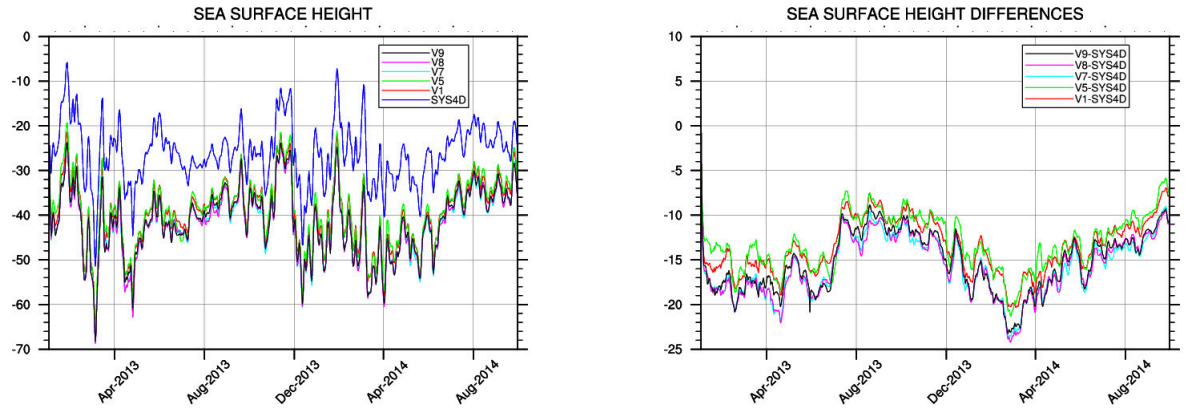

Figure 10. Sea surface height [cm] comparison (left-hand side panel) and differences between MFS sys4d and the experiments performed (right-hand side panel) for the whole period of simulation.

Figure 11 shows the sea surface current module. Experiments sys4d and V1 present lower values with respect to the other experiments performed (Figure 11, left-hand panel), while the highest values are achieved with experiment V5.

This is clear also from the right-hand panel of Figure 11, where all the experiments performed show a positive difference with respect to sys4d simulation, except V1 which oscillates around a zero difference with respect to sys4d.

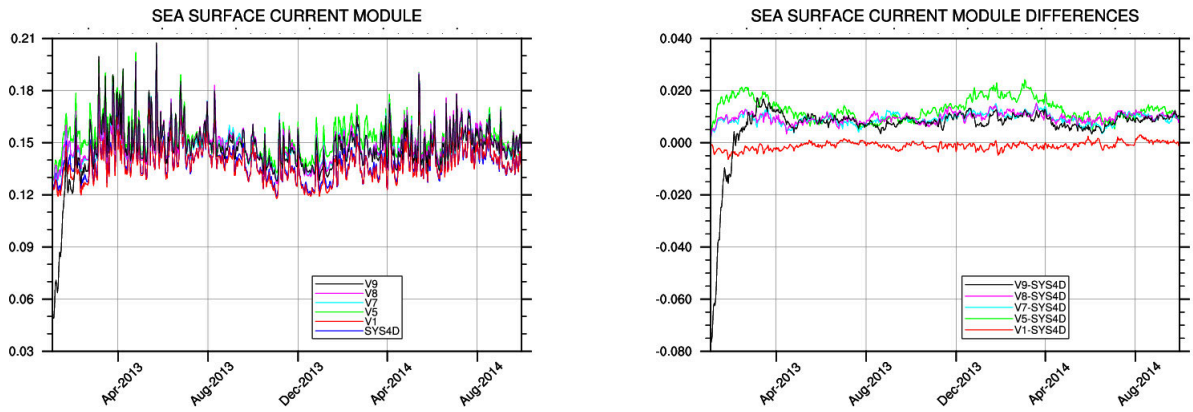

Figure 11. Sea surface current module [m/s] comparison (left-hand side panel) and differences between the experiments performed and MFS sys4d (right-hand side panel) for the whole period of simulation.

Figure 12 presents the volume averaged currents time series showing that V1 has the lowest values, V5 and V9 have the highest values, the latter converging toward the results of the other experiments after 4 months of simulation, we can also notice the presence of 3 couples of curves, sorted by increasing sea surface current module: sys4d and V1, V7 and V8, V9 and V5.

Concerning the comparison with sys4d, all the experiments performed show a positive difference with respect to sys4d, except for V1 experiment.

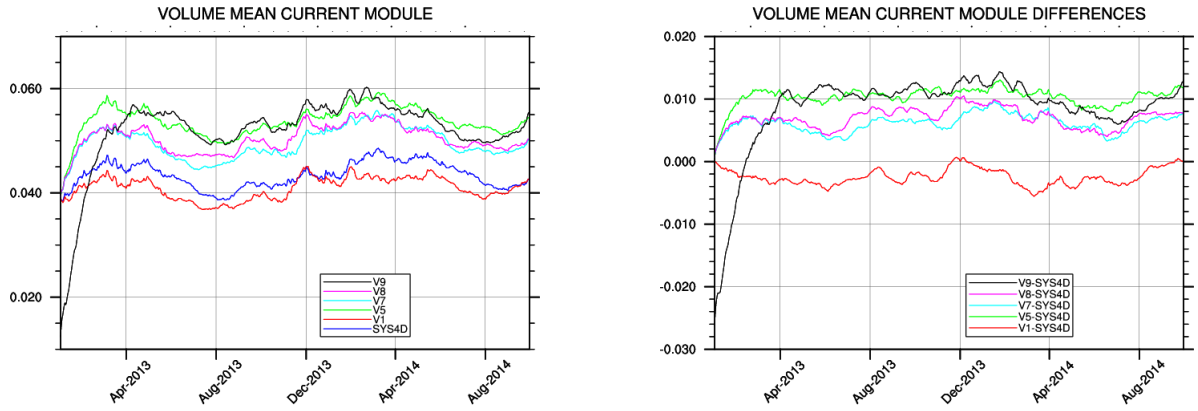

Figure 12. Volume mean current module comparison (left-hand side panel) and differences between the experiments performed and MFS sys4d (right-hand side panel) for the whole period of simulation.

4.2 Misfits (Temperature, Salinity, Sea Level Anomaly)

The misfits (observations minus model results) of the numerical model results with respect to temperature and salinity vertical ARGO profiles and along track satellite sea level anomaly (SLA) observations are presented in this paragraph. The comparison between SLA model results and observations from satellites has been carried out for the satellite missions which are assimilated through the 3D-VAR scheme used.

The comparison between model results and ARGO salinity and temperature observations is presented for specific depths, while in paragraph 4.5 the same comparison is presented for all the depths available for observations and for different sub-basins.

The satellite missions considered for SLA observations are:

- SARAL/AltiKa, a French – Indian mission started in February 2013 and whose data are available since June 2013.
- CryoSat, a European Space Agency (ESA) mission started in April 2010 mostly dedicated to measuring the thickness of polar sea ice and monitoring changes in the ice sheets that blanket Greenland and Antarctica, but also sea level data are produced and disseminated.
- Ocean Surface Topography Mission (OSTM) on the Jason-2 satellite, a joint mission started in June 2008 by four organisations: the National Oceanic and Atmospheric Administration (NOAA), the National Aeronautics and Space Administration (NASA), the France's Centre National d'Études Spatiales (CNES) and the European Organisation for the Exploitation of Meteorological Satellites (EUMETSAT).

In Figure 13 the Root Mean Square misfits of sea level anomaly between the experiments performed and the observations from the above mentioned satellite missions are presented, and the corresponding numerical values are summarized in Table 5.

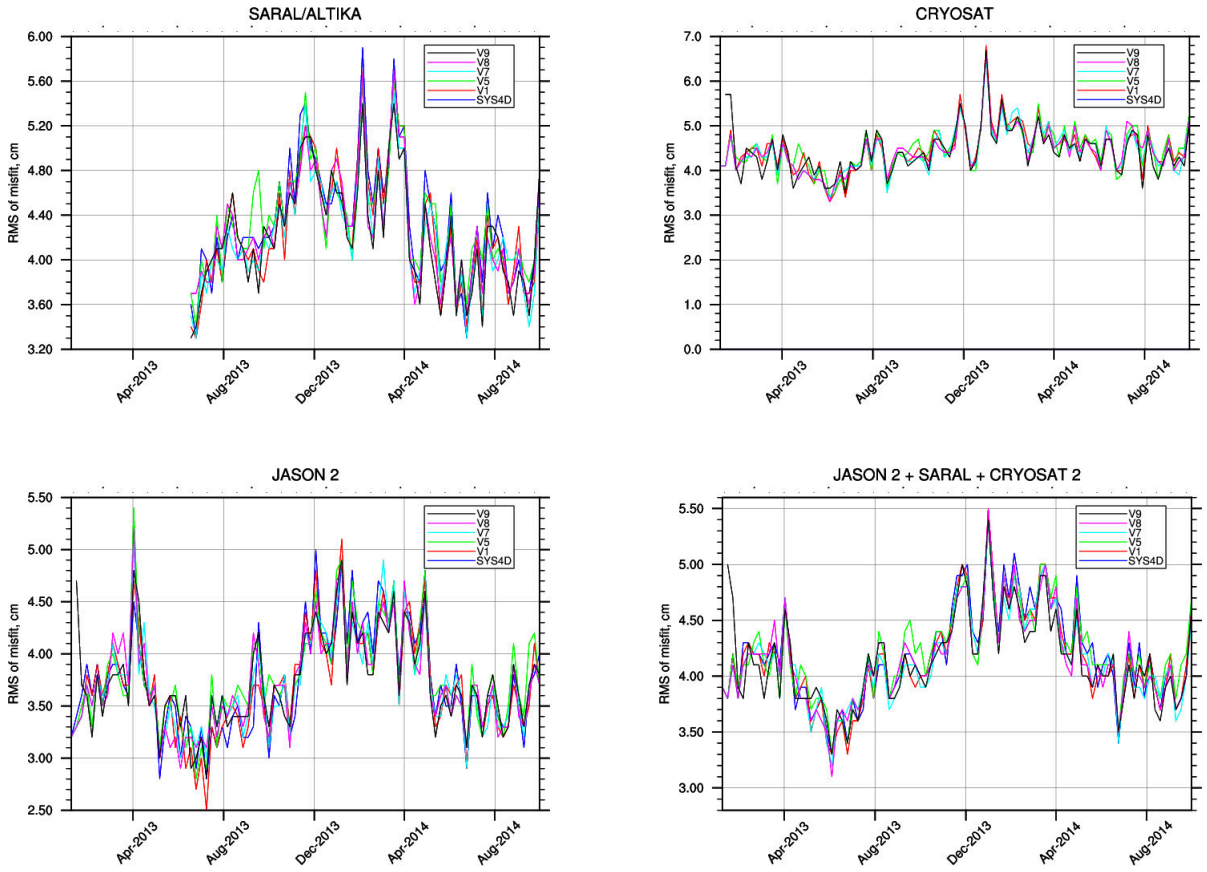

Figure 13. Root Mean Square misfits of sea level anomaly (cm) between the experiments performed and the observations from SARAL/AltiKa mission (top-left panel), CryoSat (top-right panel), OSTM/Jason-2 (bottom-left panel) and the average of the previous three ones (bottom-right).

SLA	SYS4D	V1	V5	V7	V8	V9
ALL	4.2	4.2	4.2	4.1	4.2	4.1
Altika/Saral	4.3	4.3	4.3	4.2	4.3	4.2
Cryosat	4.5	4.5	4.5	4.4	4.5	4.4
Jason2	3.7	3.7	3.8	3.7	3.7	3.7

Table 5. Root Mean Square misfits of sea level anomaly (cm) between the experiments performed and the satellite observations presented in Figure 13.

As highlighted by Figure 13, and Table 5, V7 and V9 experiment show the best performances in the comparison with SARAL/AltiKa and CryoSat observations, while for OSTM/Jason-2 observations comparison all the experiments show extremely similar results. The comparison of the numerical simulations with respect to the average of the three satellite missions considered, shows that V7 and V9 are the experiments producing the best results.

In Figure 14 the Root Mean Square misfits of temperature between the experiments performed and the observations from ARGO floats are presented, and the corresponding numerical values are summarized in Table 6.

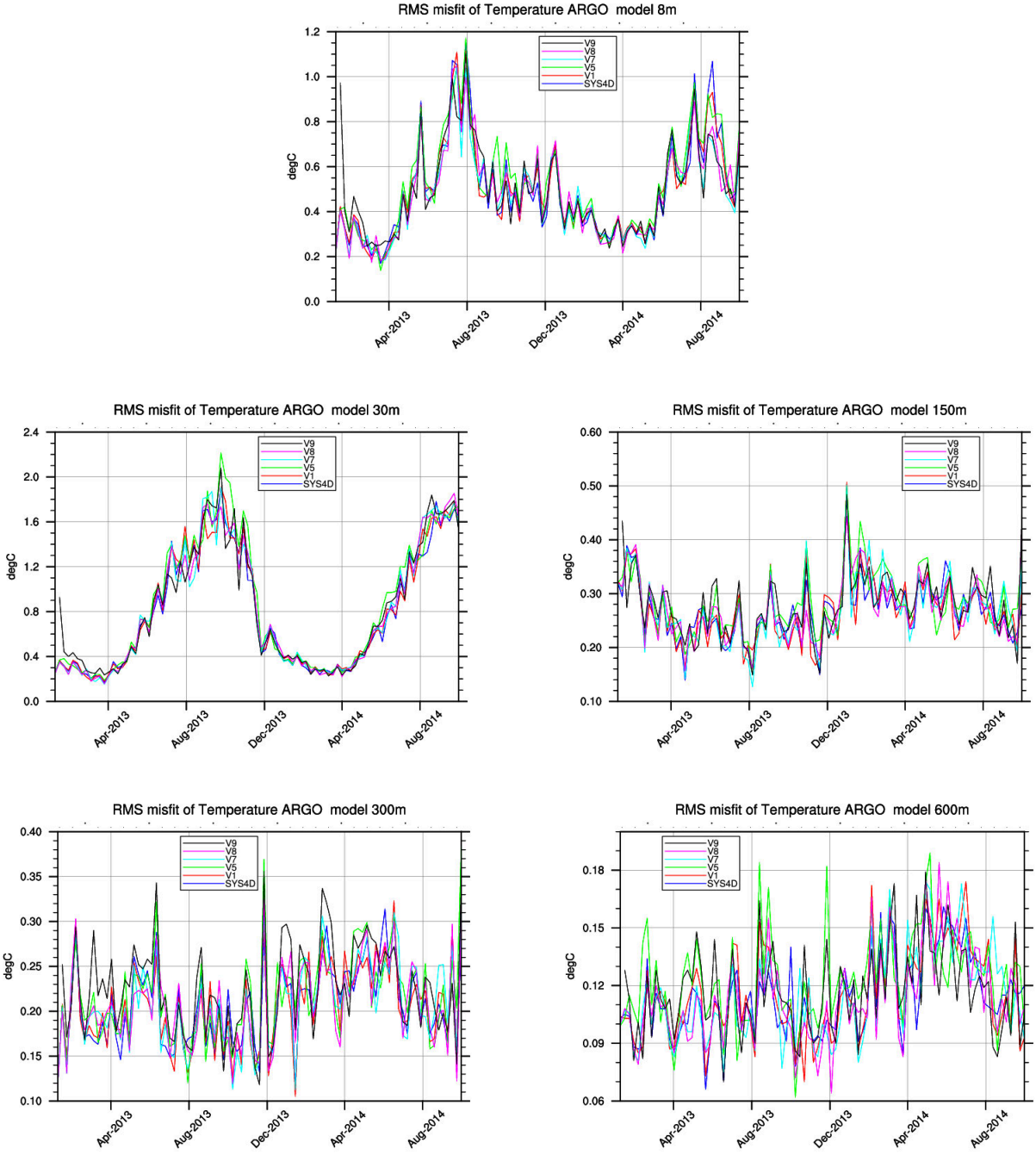

Figure 14. Root Mean Square misfits of temperature (C^o) between the experiments performed and the observations from ARGO at specific depths.

Temperature	SYS4D	V1	V5	V7	V8	V9
8 m	0.5	0.49	0.52	0.47	0.48	0.5
30 m	0.8	0.8	0.86	0.81	0.81	0.83
150 m	0.27	0.27	0.28	0.27	0.27	0.28
300 m	0.21	0.21	0.22	0.21	0.21	0.23
600 m	0.11	0.12	0.12	0.11	0.11	0.12

Table 6. Root Mean Square misfits of temperature (C^o) between the experiments performed and the ARGO floats observations presented in Figure 13.

As showed in Figure 14 and Table 6, experiment V7 presents the best performances, while V5 exhibits the worst results; the skills of experiment V9 are influenced by the climatological initial conditions (the other experiments have been initialized using the same restart from MFS sys4d operational system), as it will be discussed in the following.

In Figure 15 the Root Mean Square misfits of salinity between the experiments performed and the observations from the above mentioned satellite missions are presented, and the corresponding numerical values are summarized in Table 7.

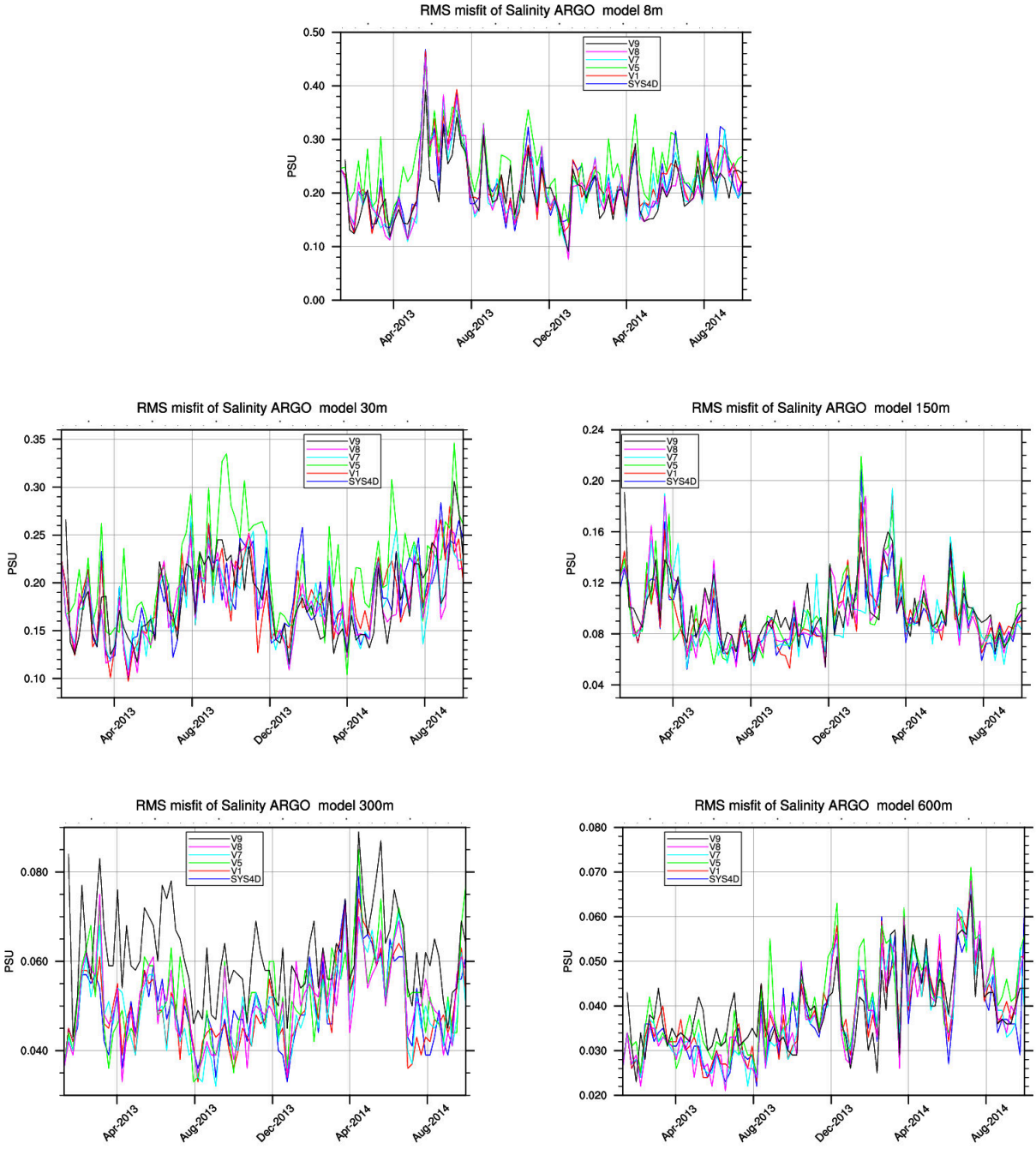

Figure 15. Root Mean Square misfits of salinity between the experiments performed and the observations from ARGO at specific depths.

Salinity	SYS4D	V1	V5	V7	V8	V9
8 m	0.22	0.22	0.24	0.21	0.21	0.2
30 m	0.19	0.18	0.21	0.18	0.18	0.18
150 m	0.09	0.09	0.1	0.09	0.1	0.1
300 m	0.05	0.05	0.05	0.05	0.05	0.06
600 m	0.04	0.04	0.04	0.04	0.04	0.04

Table 7. Root Mean Square misfits of salinity (PSU) between the experiments performed and the ARGO floats observations presented in Figure 14.

As showed in Figure 15 and Table 7, the experiment with the best results is V7, while the experiment with the worst results is V5; as for temperature, the skills of experiment V9 are influenced by the fact that it has been started from climatological initial conditions, but V9 is anyway the experiment with the best performances at surface (8 m layer).

4.3 CalVal buoys (Temperature, Salinity, Currents, Sea Surface Height)

The experiments have been validated using the CalVal (Calibration/Validation) tool developed at INGV in the framework of MyOcean project.

The purpose of the MyOcean WP9 CalVal activities is to assess the quality of the Med MFC external products, e.g. daily mean temperature, salinity, sea level and current fields, in terms of MERSEA Class 4 diagnostics.

The Class 4 metrics aim to measure, using independent in-situ observations, the performance of the forecasting system, its capability to describe the ocean (hindcast mode), as well as its forecasting skill (analysis and forecast mode).

In the following the performances of the experiments carried evaluated using CalVal tool are summarized in Table 8, and some sample comparisons are presented.

VARIABLE	V1	V5	V7	V8	V9
T	5	7	9	12	14
S	2	1	2	0	5
SSH	10	16	11	5	8

Table 8. Number of buoys for which each experiment shows the best performances, divided by variable.

The experiment V9 presents the best performances for the most part of the buoys considered, in particular for temperature and salinity observations, while for the SSH (Sea Surface Height) V5 shows the highest skill.

Zonal and meridional current data have not been taken into account in Table 8, since they are very few for the considered period.

In Figure 16 the comparison of Root Mean Square Error of temperature between all the experiments performed and MFS sys4d (labeled hereafter in pictures as MFS Currents V4 AN) is shown for the Alghero station.

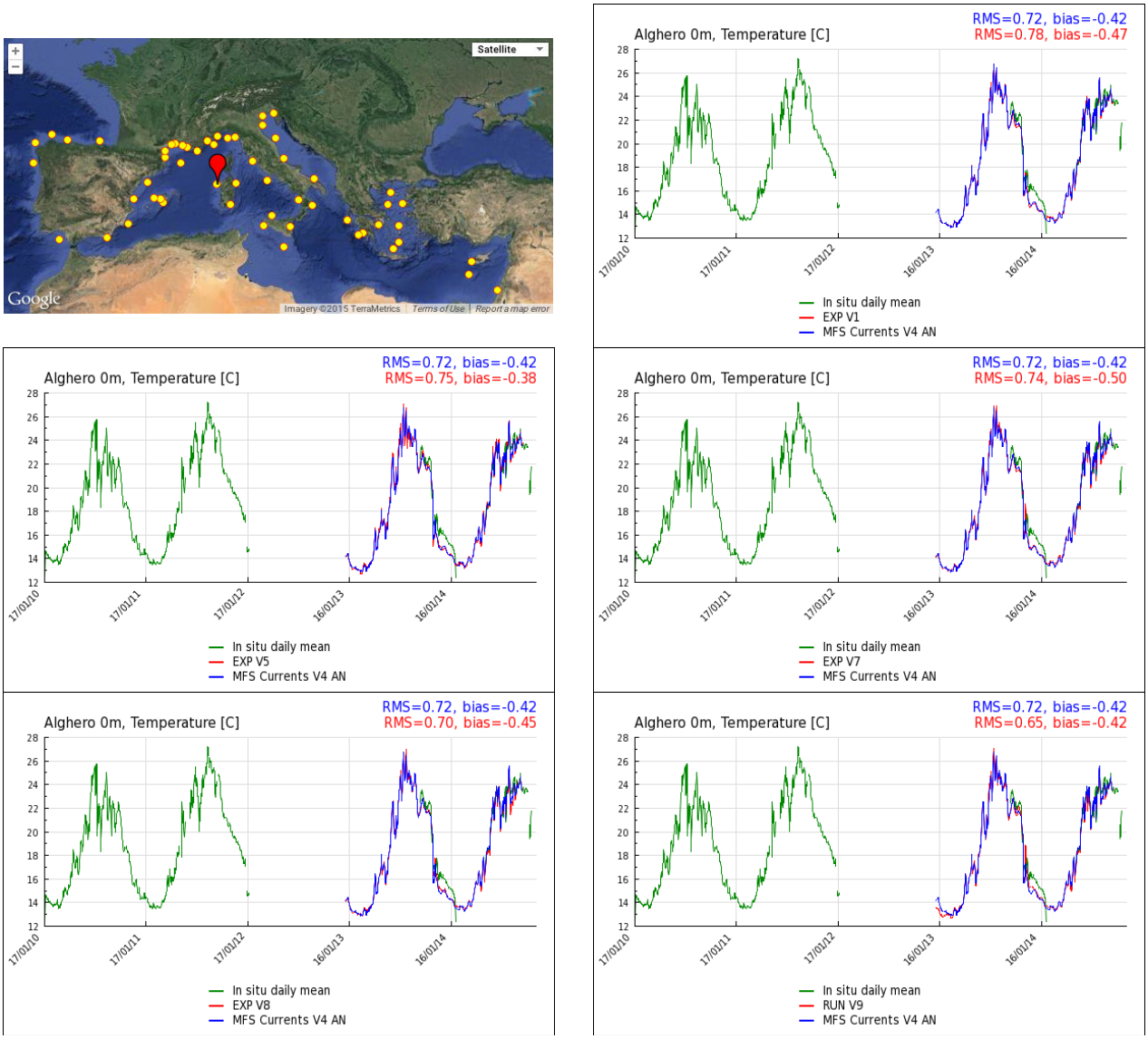

Figure 16. Root Mean Square Error of temperature at surface of the performed experiments at Alghero station.

Considering the Alghero buoy station, all the experiments show a higher temperature RMSE with respect to MFS sys4d, with the exception of experiment V8 and experiment V9, the latter showing an improvement of 10% in temperature representation with respect to MFS sys4d.

In Figure 17 the comparison of salinity RMSE at 3 m depth between all the experiments and MFS sys4d run is shown for Cabo de Palos buoy station.

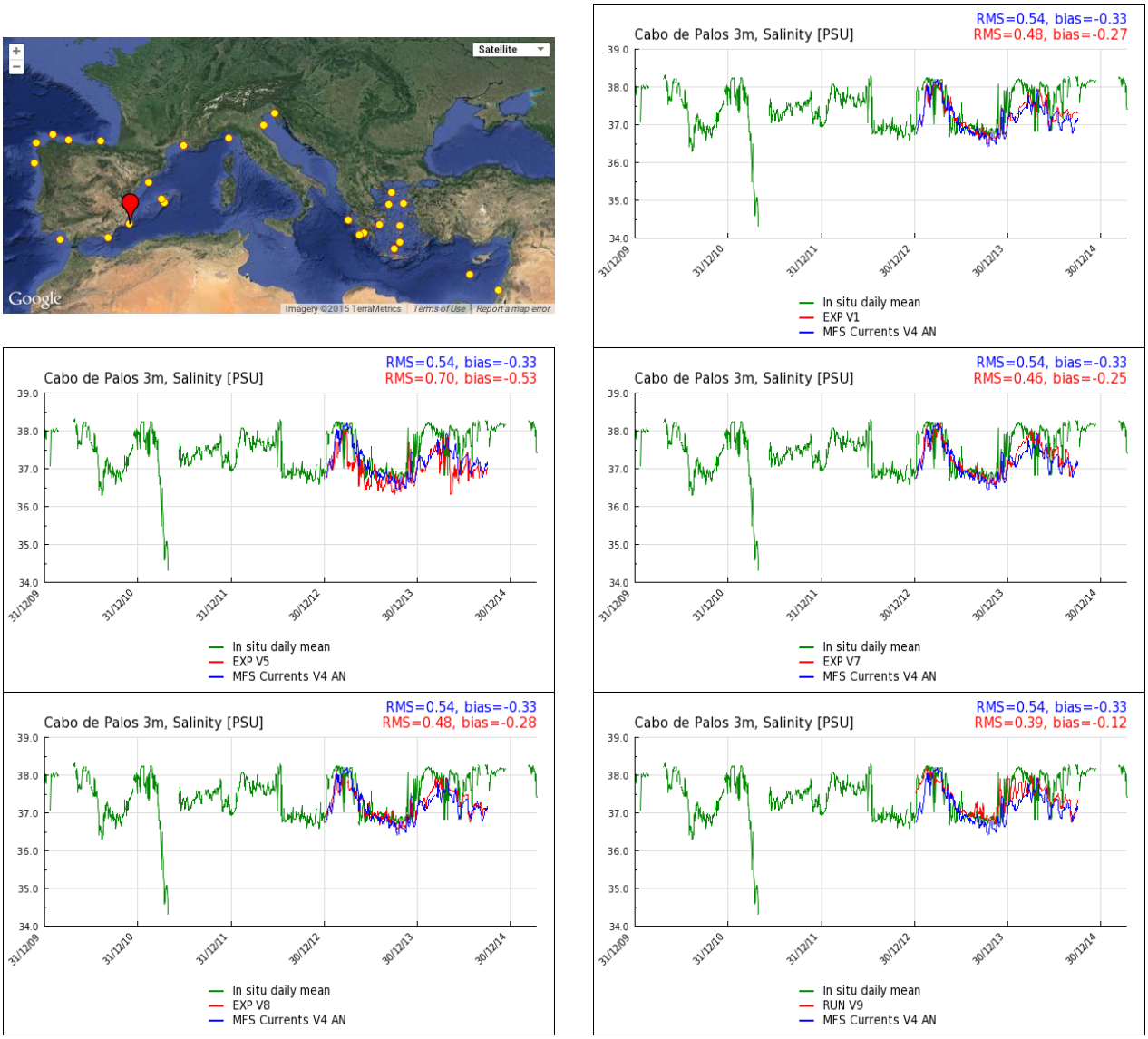

Figure 17. Root Mean Square Error of salinity at 3 m depth of the performed experiments at Cabo de Palos station.

For Cabo de Palos station all the experiments performed show a lower RMSE of salinity with respect to MFS sys4d, with the exception of experiment V5, which shows a worsening of 22%. Experiments V7 and V9 show the best results, with an improvement of 15% and 28% respectively compared to MFS sys4d.

In Figure 18 the comparison of sea surface height RMSE between all the experiments performed and MFS sys4d run is shown for the Vieste buoy. All the experiments performed show a lower RMSE with respect to MFS sys4d, with an improvement ranging from a minimum of 12% in experiment V8 to a maximum of 16% in experiment V1.

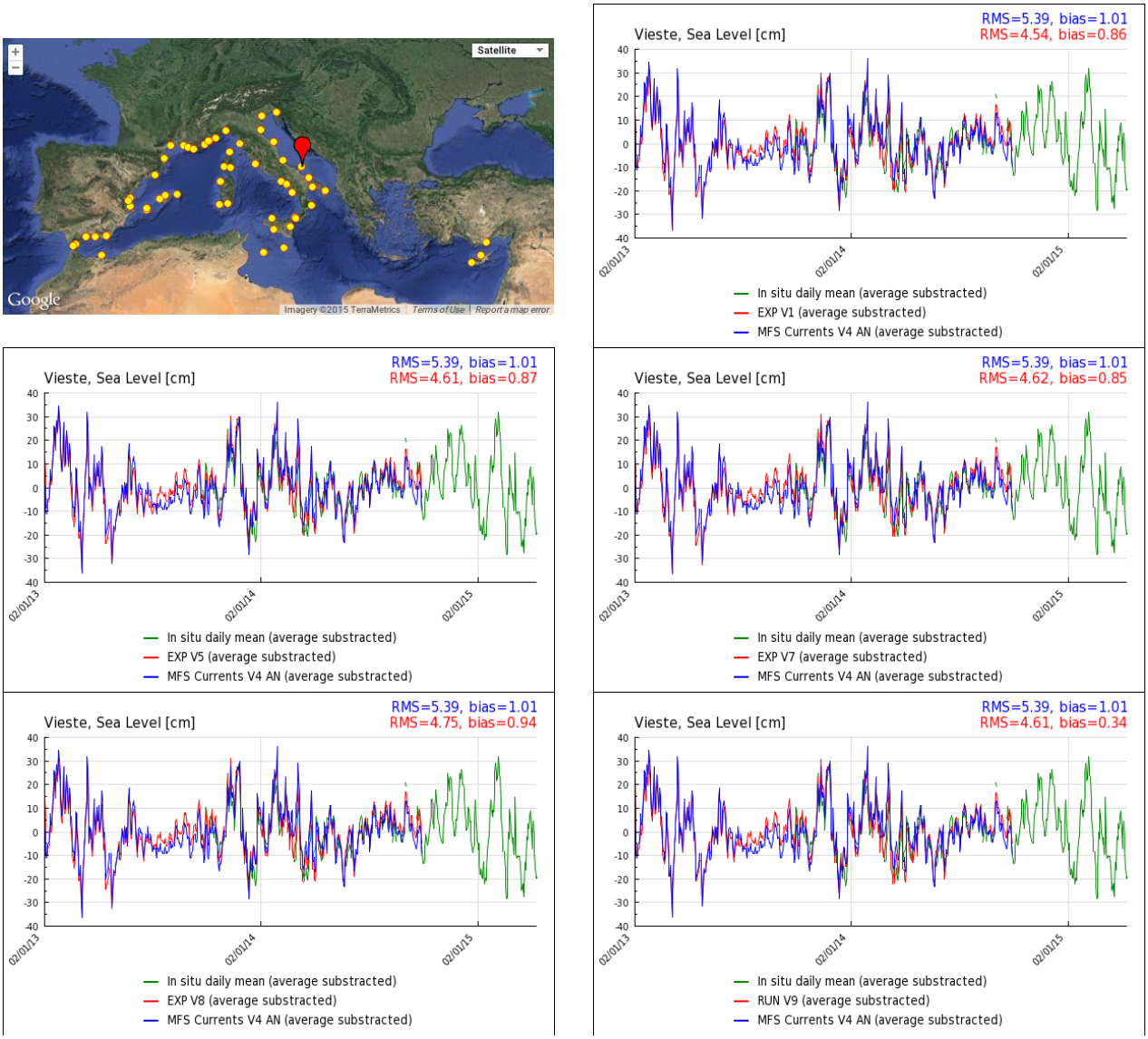

Figure 18. Root Mean Square Error of sea surface height of the performed experiments at Vieste station.

In Figure 19 the comparison of zonal current RMSE between all the experiments performed and MFS sys4d run is shown for Tarragona buoy station. Most of the experiments performed show a lower zonal current RMSE with respect to MFS sys4d, with an improvement ranging from a minimum of 0.3% in experiment V8 to a maximum of 5% in experiment V9.

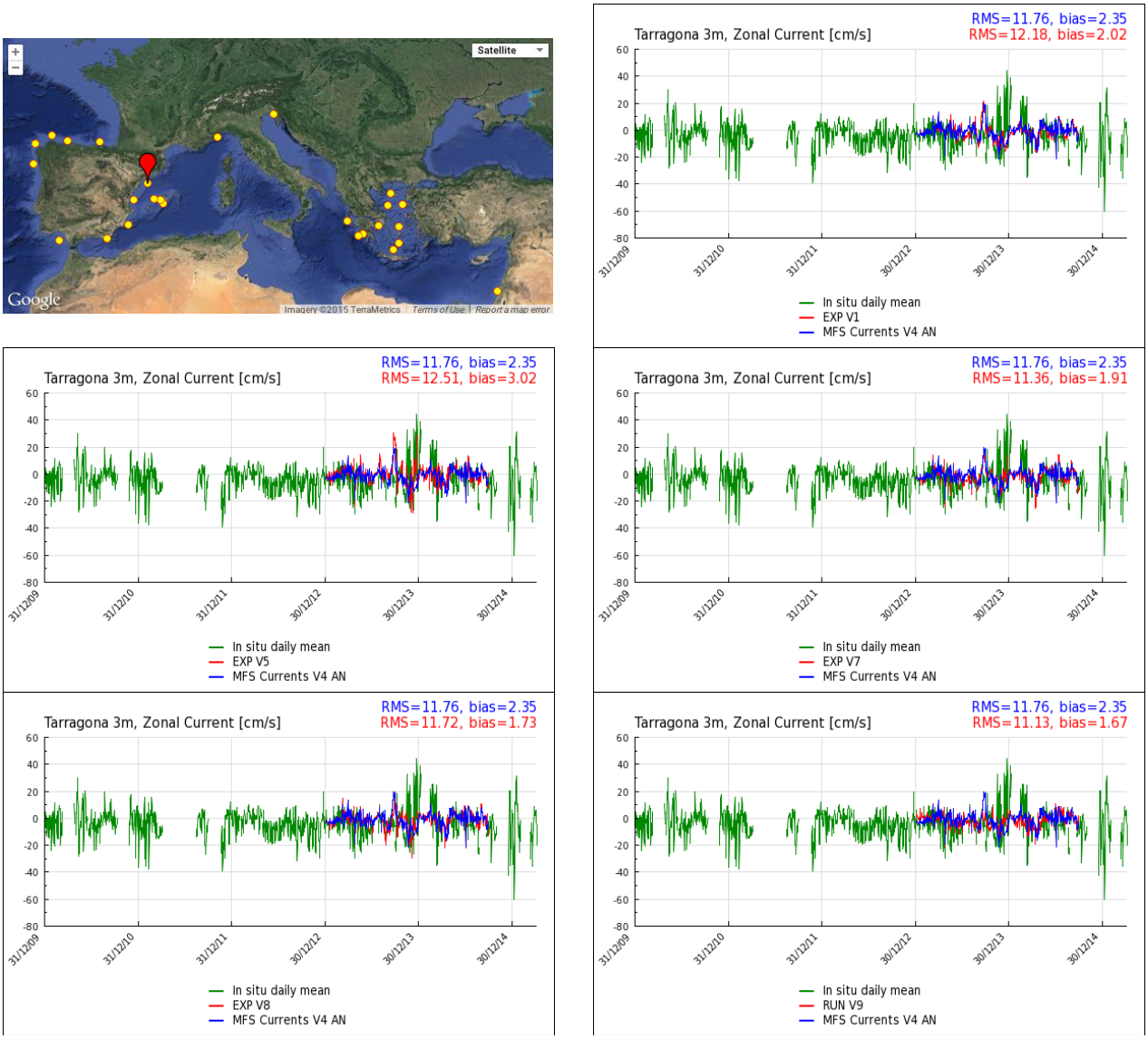

Figure 19. Root Mean Square Error of zonal current at 3 m depth of the performed experiments at Tarragona station.

In Figure 20 the comparison of meridional current RMSE between all the experiments performed and MFS sys4d run is shown for Tarragona buoy station. All the experiments performed show a lower meridional current RMSE with respect to MFS sys4d, with an improvement ranging from a minimum of 1.5% in experiment V1 to a maximum of 25% in experiment V5. Also experiment V9 shows a large improvement with respect to MFS sys4d (about 17%).

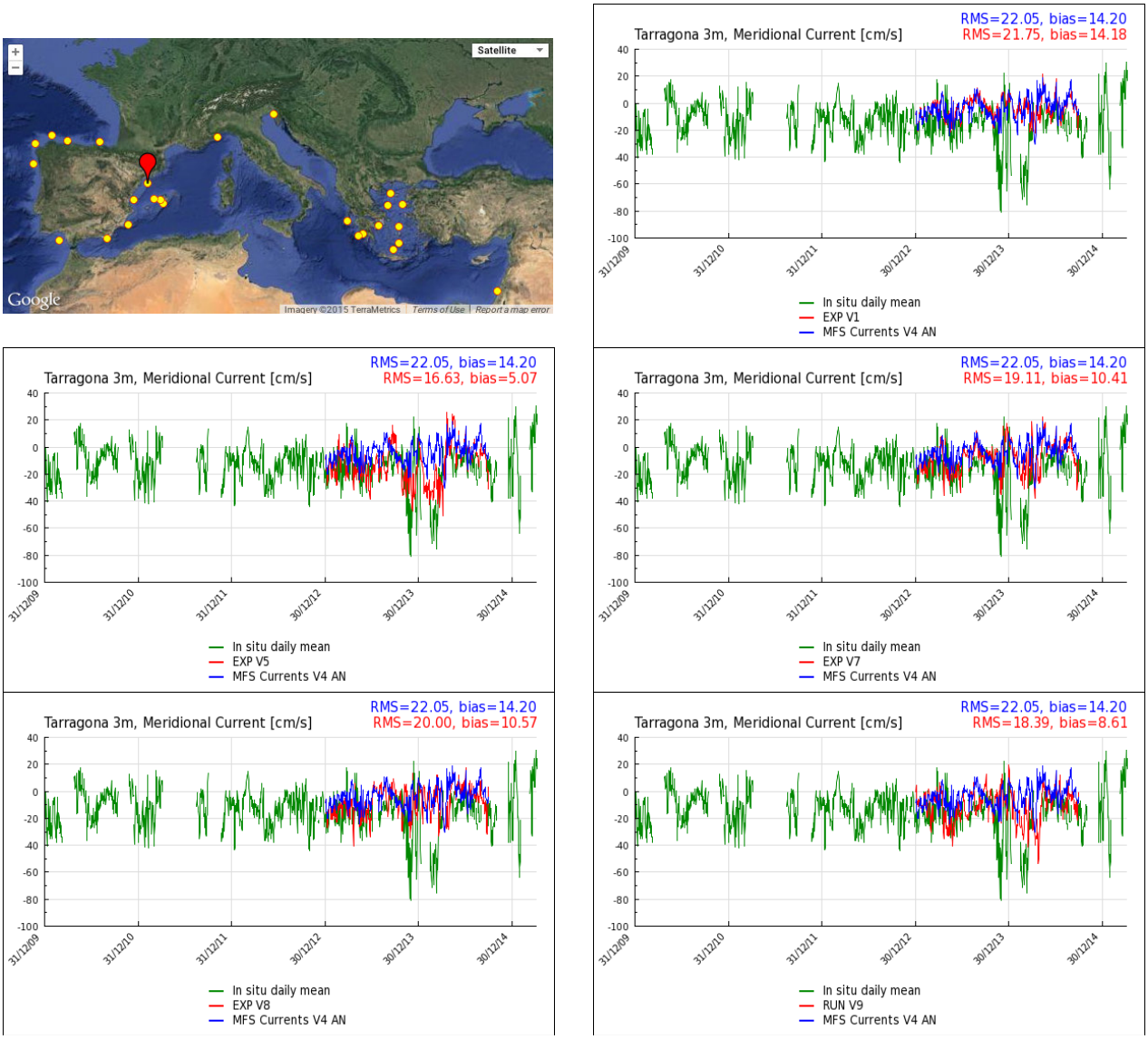

Figure 20. Root Mean Square Error of meridional current at 3 m depth of the performed experiments at Tarragona station.

4.4 Estimated Accuracy Numbers (Temperature, Salinity, Sea Surface Temperature, Sea Level Anomaly)

Estimated Accuracy Numbers (EANs) are a standard developed within MyOcean project for providing accuracy metrics for a wide range of products to the users.

EANs have been calculated for each experiment, in order to give an overview of the performances of the different setups used.

The Mediterranean basin has been subdivided into 13 different regions (Figure 21), and the computation of EANs has been performed for each of them and for the entire basin.

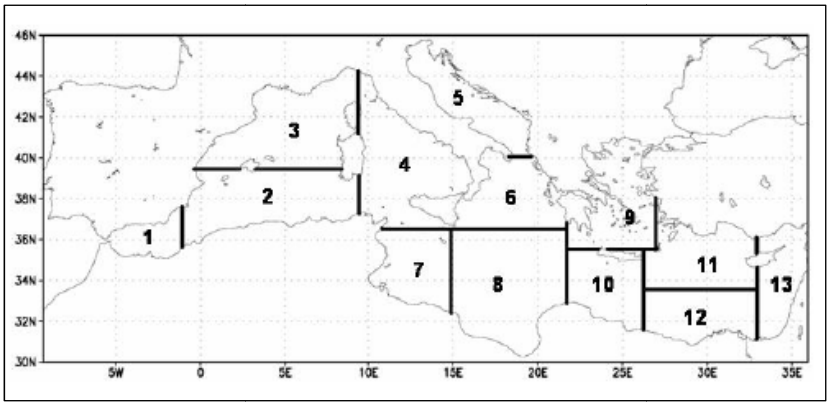

Figure 21. Mediterranean basin subdivision for Estimated accuracy number computation.

In the following the tables containing the EANs for each region are presented; "MISFIT" is defined as Observation – Model, while "RMS" is the Root Mean Square Error. The vertical layers considered are:

- 1 Layer: 0 – 10 m.
- 2 Layer: 10 – 30 m.
- 3 Layer: 30 – 150 m.
- 4 Layer: 150 – 300 m.
- 5 Layer: 300 – 600 m.
- 6 Layer: 600 – 1000 m.

Figures 22-23 show respectively histograms of temperature and salinity EANs evaluated for the entire basin and for each region at different vertical layers.

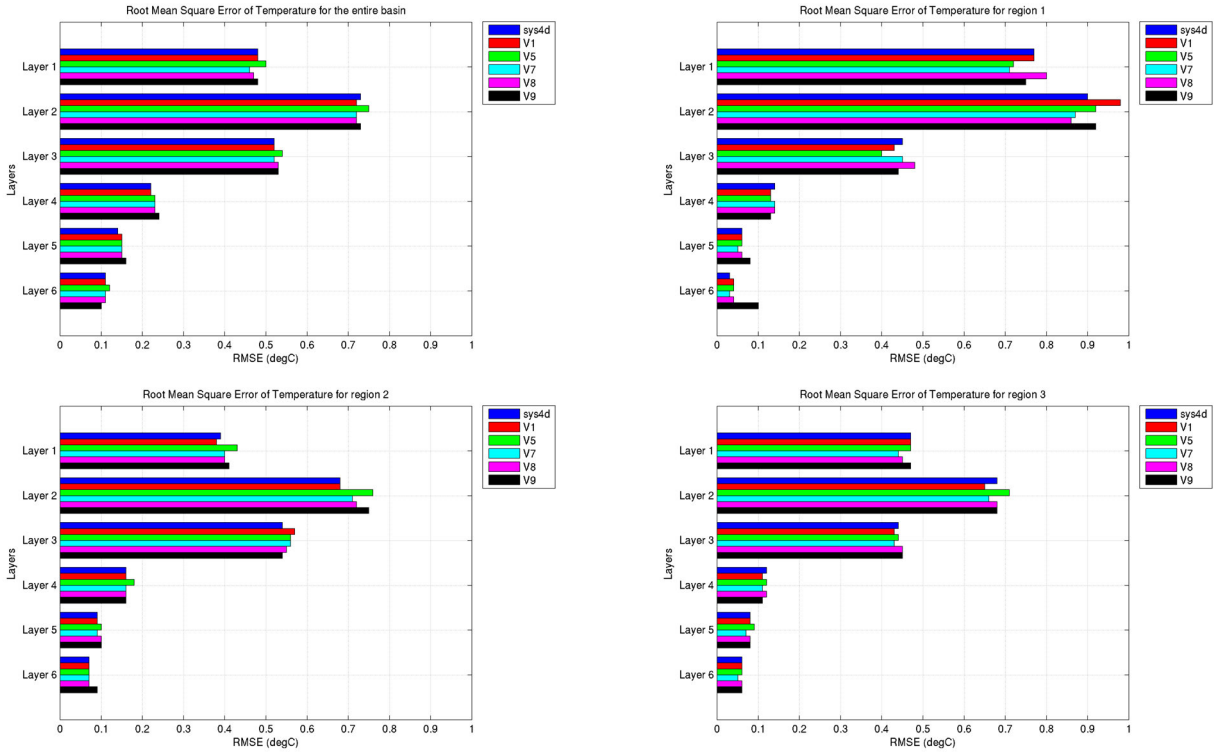

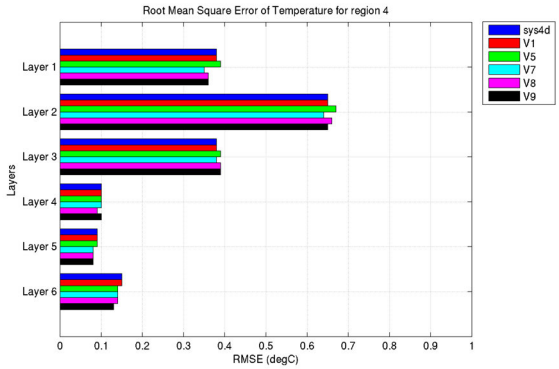
Root Mean Square Error of Temperature for region 4
sys4d
V1
V5
V7
V8
V9
Layer 1
Layer 2
Layer 3
Layer 4
Layer 5
Layer 6
Layers
0 0.1 0.2 0.3 0.4 0.5 0.6 0.7 0.8 0.9 1
RMSE (degC)

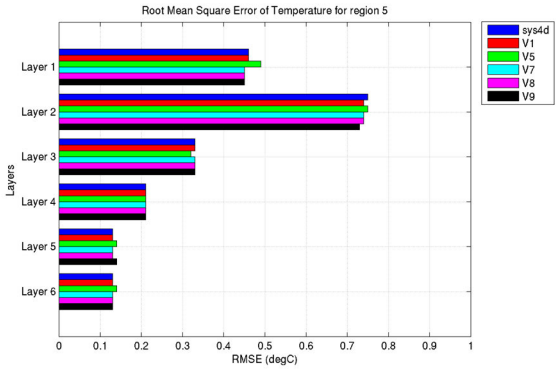
Root Mean Square Error of Temperature for region 5
sys4d
V1
V5
V7
V8
V9
Layer 1
Layer 2
Layer 3
Layer 4
Layer 5
Layer 6
Layers
0 0.1 0.2 0.3 0.4 0.5 0.6 0.7 0.8 0.9 1
RMSE (degC)

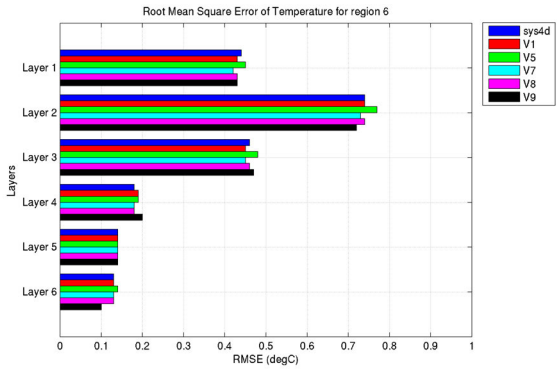
Root Mean Square Error of Temperature for region 6
sys4d
V1
V5
V7
V8
V9
Layer 1
Layer 2
Layer 3
Layer 4
Layer 5
Layer 6
Layers
0 0.1 0.2 0.3 0.4 0.5 0.6 0.7 0.8 0.9 1
RMSE (degC)

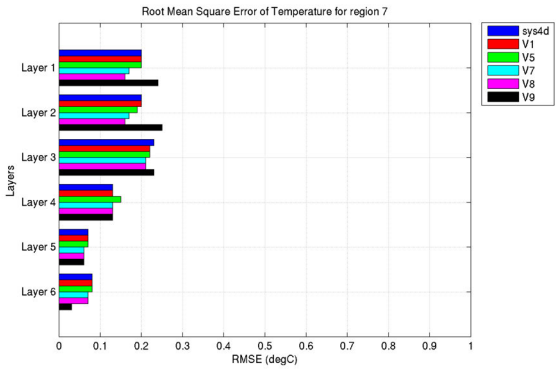
Root Mean Square Error of Temperature for region 7
sys4d
V1
V5
V7
V8
V9
Layer 1
Layer 2
Layer 3
Layer 4
Layer 5
Layer 6
Layers
0 0.1 0.2 0.3 0.4 0.5 0.6 0.7 0.8 0.9 1
RMSE (degC)

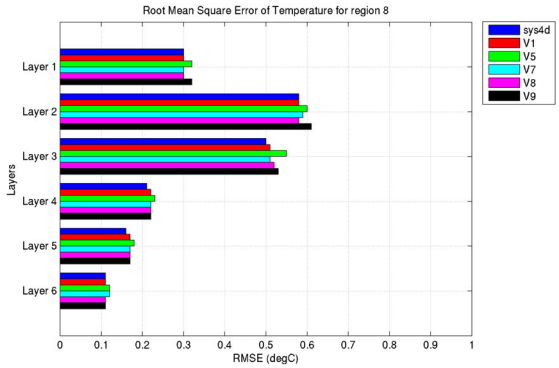
Root Mean Square Error of Temperature for region 8
sys4d
V1
V5
V7
V8
V9
Layer 1
Layer 2
Layer 3
Layer 4
Layer 5
Layer 6
Layers
0 0.1 0.2 0.3 0.4 0.5 0.6 0.7 0.8 0.9 1
RMSE (degC)

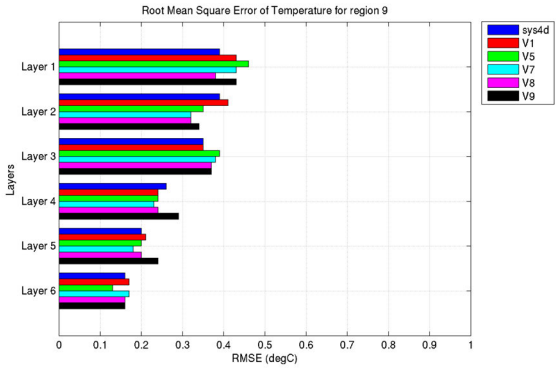
Root Mean Square Error of Temperature for region 9
sys4d
V1
V5
V7
V8
V9
Layer 1
Layer 2
Layer 3
Layer 4
Layer 5
Layer 6
Layers
0 0.1 0.2 0.3 0.4 0.5 0.6 0.7 0.8 0.9 1
RMSE (degC)

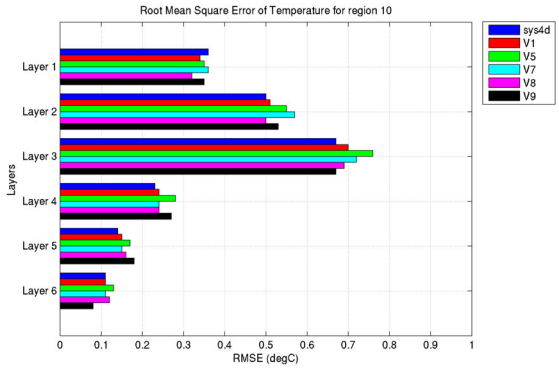
Root Mean Square Error of Temperature for region 10
sys4d
V1
V5
V7
V8
V9
Layer 1
Layer 2
Layer 3
Layer 4
Layer 5
Layer 6
Layers
0 0.1 0.2 0.3 0.4 0.5 0.6 0.7 0.8 0.9 1
RMSE (degC)

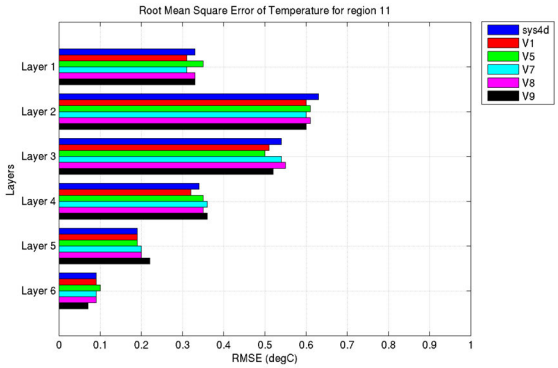
Root Mean Square Error of Temperature for region 11
sys4d
V1
V5
V7
V8
V9
Layer 1
Layer 2
Layer 3
Layer 4
Layer 5
Layer 6
Layers
0 0.1 0.2 0.3 0.4 0.5 0.6 0.7 0.8 0.9 1
RMSE (degC)

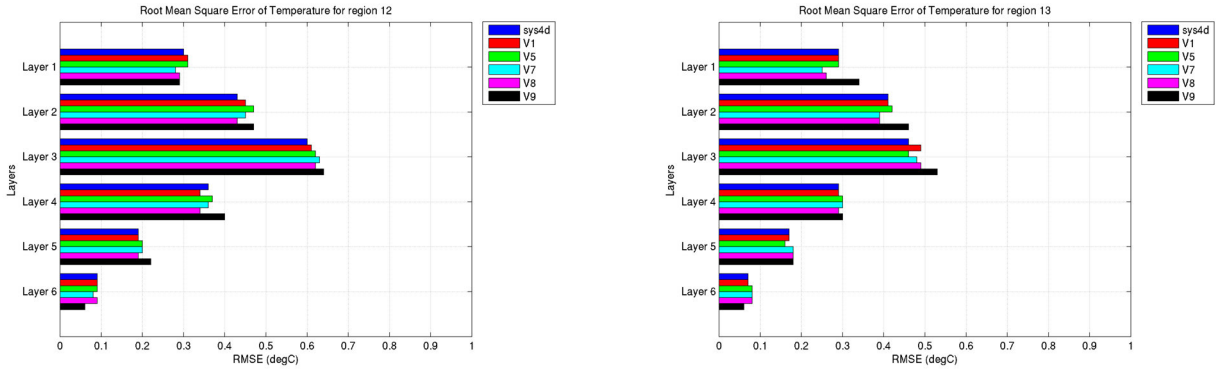

Figure 22. Temperature Estimated accuracy number for the entire basin and for the regions defined.

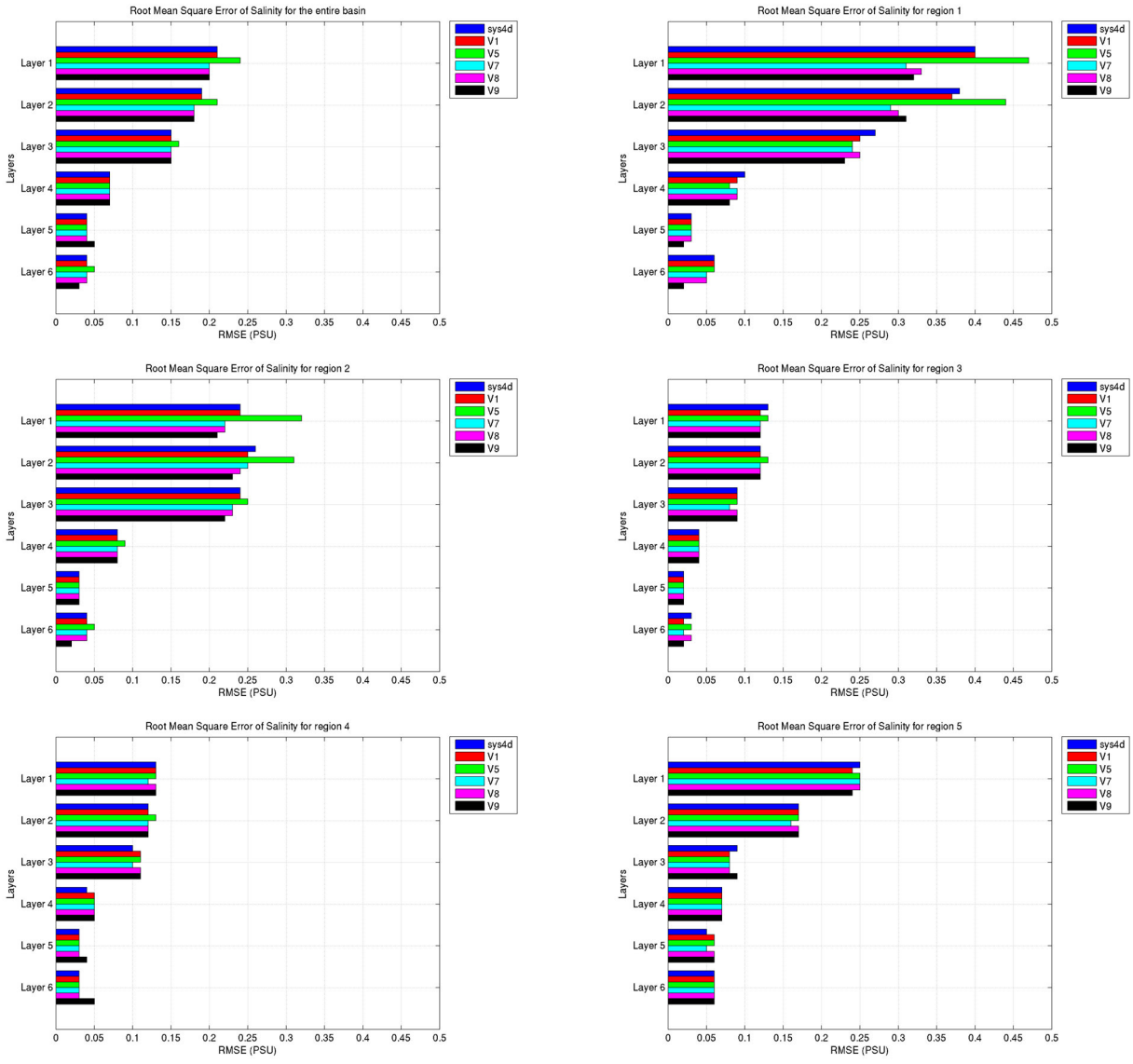

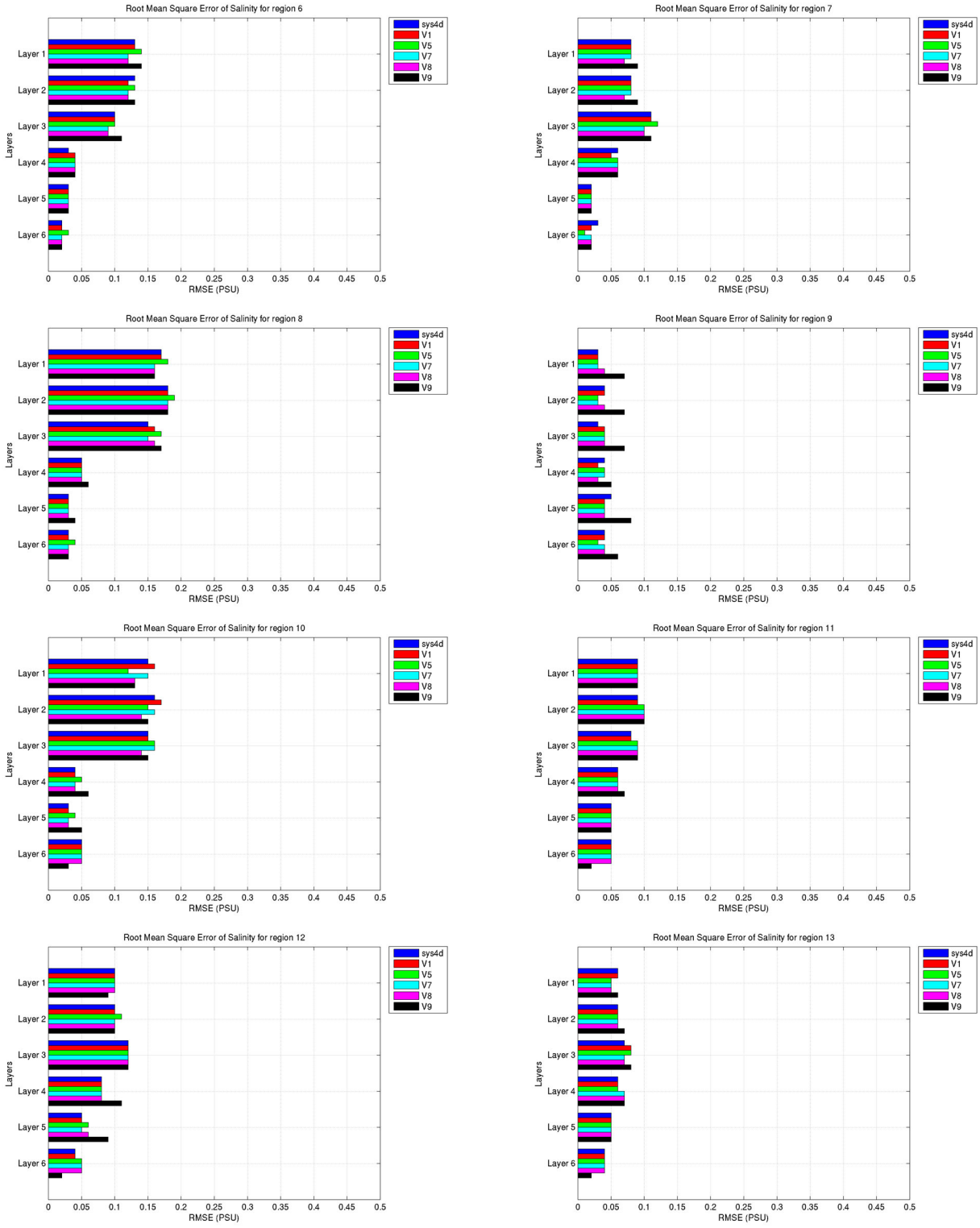

Figure 23. Salinity Estimated accuracy number for the entire basin.

As presented in Figure 22, the EANs show that for temperature for the entire basin in the first two layers (0 – 30 m depth) the V7 experiment has the best performances, while at intermediate depths (150 – 600 m) the sys4d and the V1 experiments perform better; at the bottom (600 – 1000 m depth) the V9 experiment shows the best skill.

The V7 experiment shows the best results in most of the sub-regions considered, in particular in the Layer 1 (from surface to 10 m depth) and, to a lesser extent, in Layer 2 (from 10 to 30 m depth).

Also the experiment V8 shows a good behavior in the same layers as for V7 experiment, while the experiment V5 shows the worst results.

For salinity (Figure 23), the EANs show that for the entire basin the experiments with the best results are V7, V8 and V9, in particular in Layer 1 and 2 for many of the sub-regions considered.

The V5 experiment has the worst results, in particular for the first three vertical layers.

In Table 9 the EANs sea level anomaly (SLA) and for the sea surface temperature (SST) calculated for the entire basin and for each region are shown.

SLA	SYS4d	V1	V5	V7	V8	V9
	RMS	RMS	RMS	RMS	RMS	RMS
MED SEA	4.3	4.3	4.4	4.3	4.3	4.3
REGION 1	4.8	4.8	4.9	4.8	4.8	4.8
REGION 2	4.7	4.7	4.9	4.7	4.8	4.6
REGION 3	3.5	3.4	3.4	3.4	3.5	3.4
REGION 4	3.4	3.4	3.4	3.4	3.4	3.4
REGION 5	2.5	2.6	2.5	2.5	2.5	2.5
REGION 6	3.1	3.2	3.1	3.1	3.1	3
REGION 7	3.1	3.1	3.1	3.1	3.1	3.1
REGION 8	3.4	3.4	3.4	3.4	3.3	3.3
REGION 9	3.4	3.4	3.4	3.4	3.4	3.3
REGION 10	3.4	3.4	3.6	3.5	3.4	3.4
REGION 11	3.2	3.1	3.3	3.2	3.3	3.3
REGION 12	3.7	3.6	3.7	3.6	3.6	3.7
REGION 13	3.1	3.1	3.1	3.1	3.1	3.2

	SYS4d	V1	V5	V7	V8	V9
SST	RMS	RMS	RMS	RMS	RMS	RMS
MED SEA	0.5	0.5	0.5	0.49	0.49	0.55
REGION 1	0.66	0.63	0.63	0.69	0.69	0.74
REGION 2	0.44	0.44	0.44	0.43	0.43	0.49
REGION 3	0.49	0.49	0.49	0.48	0.48	0.52
REGION 4	0.44	0.43	0.43	0.43	0.43	0.48
REGION 5	0.57	0.58	0.58	0.57	0.58	0.64
REGION 6	0.48	0.48	0.48	0.47	0.48	0.53
REGION 7	0.57	0.57	0.57	0.55	0.55	0.58
REGION 8	0.44	0.44	0.44	0.43	0.43	0.46
REGION 9	0.57	0.57	0.57	0.56	0.56	0.64
REGION 10	0.43	0.43	0.43	0.44	0.44	0.51
REGION 11	0.49	0.48	0.48	0.48	0.48	0.55
REGION 12	0.41	0.42	0.42	0.41	0.41	0.45
REGION 13	0.42	0.42	0.42	0.42	0.42	0.48

Table 9. Sea level anomaly (upper panel) and sea surface temperature (lower panel) Estimated accuracy number for the entire basin: in green the best skills, in red the worst skills.

For the sea level anomaly, the EANs (Table 9, left panel) show that the experiments with the best results are V7 and V9. In particular V9 has the best skills among the performed experiments in the western and central part of the Mediterranean Sea, while it has the worst performances in the eastern part of the basin. The experiment with the worst skills is V5.

For the sea surface temperature, the EANs (Table 9, right panel) show that the experiment with the best results is V7, while V9 experiment has the worst behavior among the performed experiments for all the sub-regions considered.

It has to be highlighted that, if year 2013 is considered as spin-up time, and the RMSE for temperature, salinity, sea level anomaly and sea surface temperature are recomputed only considering year 2014, a clear improvement of the V9 experiment performances is achieved. Indeed the temperature RMSE for each layer is lower with respect to the other experiments RMSE (Figure 24, left panel) and also the salinity RMSE is reduced for every layer (Figure 24, right panel).

A big improvement of experiment V9 for year 2014 is evident for sea level anomaly and sea surface temperature as shown in Table 6, confirming that the lower performances shown for the entire simulation period are due to the spin-up time.

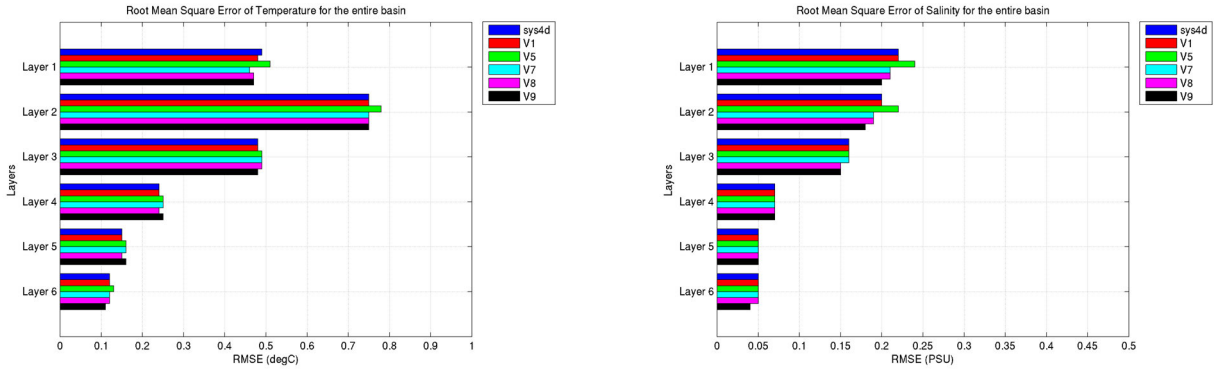

Figure 24. Temperature Estimated accuracy number for the entire basin for year 2014 (left panel), salinity Estimated accuracy number for the entire basin for year 2014 (right panel).

SLA	SYS4d	V1	V5	V7	V8	V9
	RMS	RMS	RMS	RMS	RMS	RMS
MED SEA	4.4	4.4	4.4	4.3	4.3	4.3
REGION 1	4.9	5	4.8	4.7	4.8	4.6
REGION 2	4.7	4.6	4.7	4.5	4.6	4.5
REGION 3	3.4	3.3	3.3	3.3	3.3	3.3
REGION 4	3.5	3.5	3.5	3.4	3.4	3.4
REGION 5	2.7	2.7	2.6	2.6	2.7	2.6
REGION 6	3.2	3.3	3.2	3.2	3.2	3
REGION 7	3.1	3.2	3.2	3.2	3.2	3.2
REGION 8	3.4	3.4	3.4	3.4	3.3	3.3
REGION 9	3.4	3.4	3.5	3.5	3.5	3.4
REGION 10	3.4	3.5	3.7	3.5	3.5	3.4
REGION 11	3.2	3.1	3.3	3.3	3.3	3.3
REGION 12	3.5	3.5	3.6	3.4	3.5	3.6
REGION 13	3.1	3.1	3.2	3.1	3.1	3.2

SST	SYS4d	V1	V5	V7	V8	V9
	RMS	RMS	RMS	RMS	RMS	RMS
MED SEA	0.48	0.48	0.5	0.47	0.47	0.47
REGION 1	0.69	0.67	0.65	0.71	0.7	0.69
REGION 2	0.41	0.42	0.43	0.41	0.4	0.4
REGION 3	0.47	0.47	0.49	0.46	0.46	0.46
REGION 4	0.41	0.41	0.43	0.39	0.39	0.4
REGION 5	0.53	0.54	0.56	0.53	0.54	0.53
REGION 6	0.48	0.48	0.5	0.47	0.48	0.48
REGION 7	0.55	0.55	0.56	0.53	0.53	0.53
REGION 8	0.43	0.43	0.45	0.42	0.42	0.41
REGION 9	0.55	0.55	0.57	0.55	0.55	0.51
REGION 10	0.41	0.41	0.42	0.41	0.41	0.42
REGION 11	0.44	0.43	0.47	0.43	0.43	0.42
REGION 12	0.4	0.4	0.42	0.39	0.39	0.39
REGION 13	0.4	0.39	0.42	0.39	0.39	0.39

Table 10. Sea level anomaly (upper panel) and sea surface temperature (lower panel) Estimated accuracy number for the entire basin for year 2014: in green the best skills, in red the worst skills.

4.5 ARGO Profiles

Model results have been validated using data from ARGO floats. Root Mean Square Error (RMSE) and BIAS have been computed for the entire basin and for the three sub-basins shown in Figure 25. Statistics have been evaluated separately for the whole simulation period and for year 2014 only in order to highlight the impact of two different initial conditions: operational restart file from MFS sys4d or climatological initial conditions (only for V9 experiment).

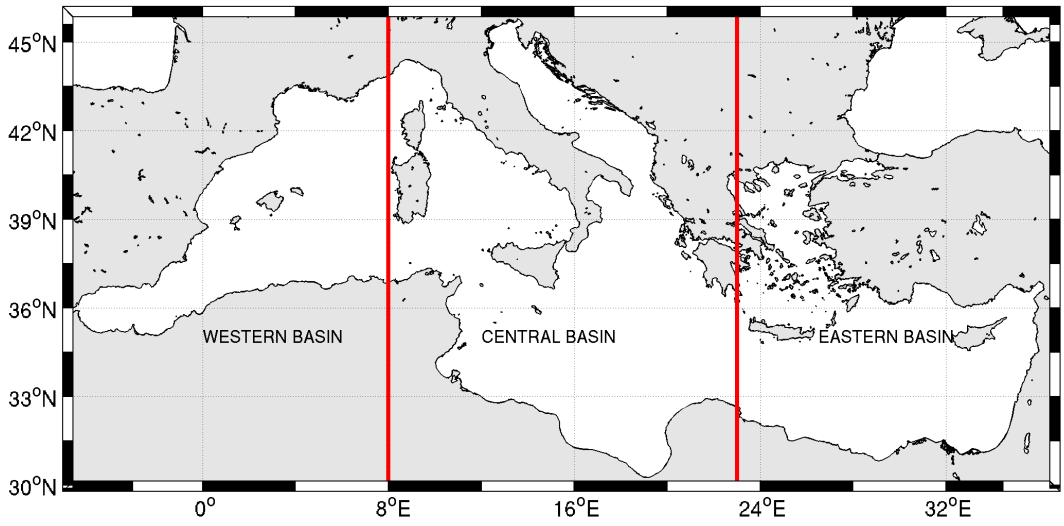

Figure 25. Basin subdivision used to compute RMSE and BIAS.

ARGO data (whose position is shown in Figure 26) have been compared with temperature and salinity numerical results at the model grid point closest to the observation; in the vertical, model values have been linearly interpolated on the observation depths.

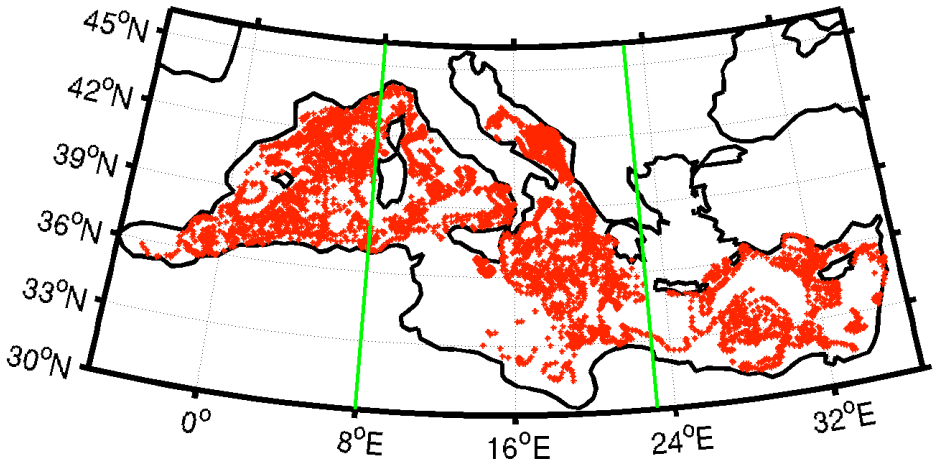

Figure 26. Location of ARGO used in the numerical experiments validation and subdivision of the entire basin in three sub-basins.

The temperature (°C) and salinity (PSU) RMSE and BIAS, averaged on the entire basin, are shown in Figures 27 and 28 respectively, where on the left hand side results are computed on the entire period of simulation, while on the right hand side only year 2014 is considered.

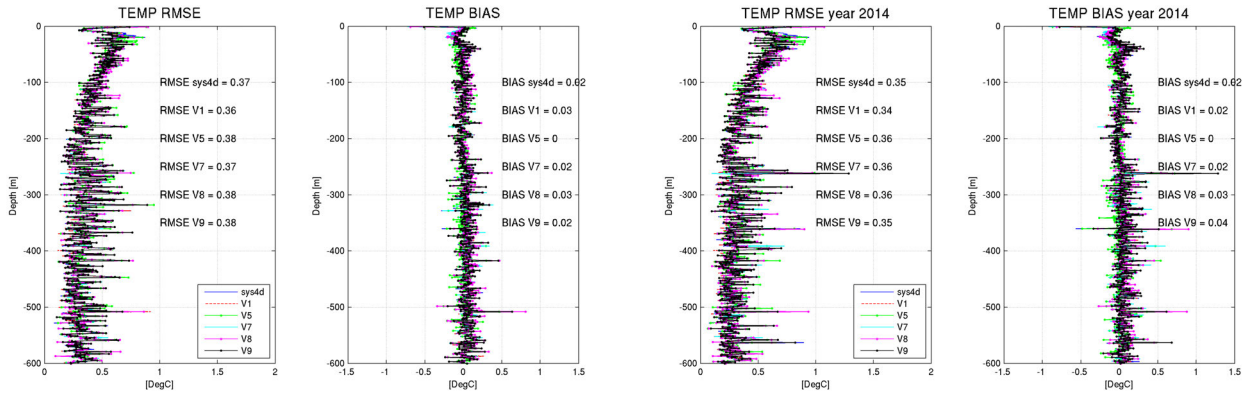

Figure 27. Root Mean Square Error (RMSE) and BIAS of temperature (°C) averaged on the entire basin for the whole simulation period (left-hand side panel) and for year 2014 only (right-hand side panel).

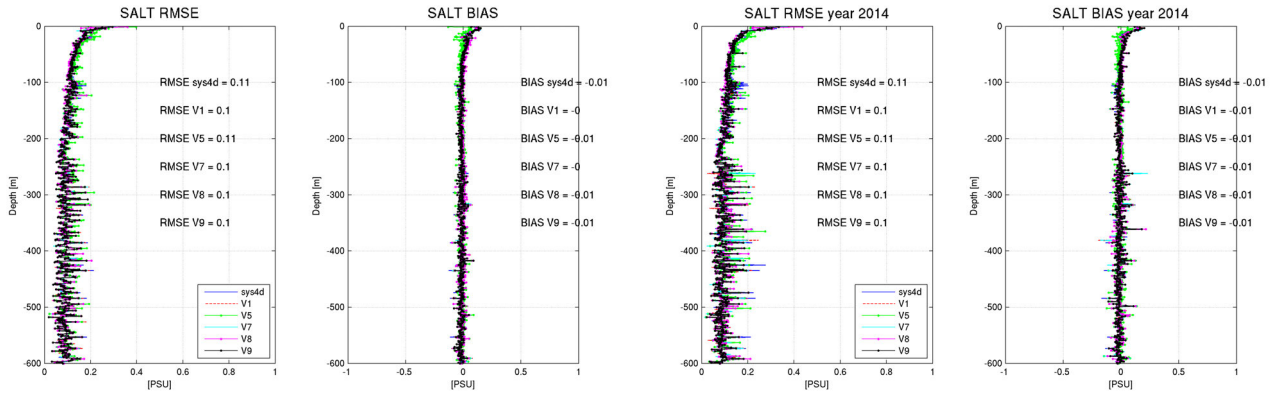

Figure 28. Root Mean Square Error (RMSE) and BIAS of salinity (PSU) averaged on the entire basin for the whole simulation period (left-hand side panel) and for year 2014 only (right-hand side panel).

The comparison with ARGO temperature observations, averaged in the entire basin, shows similar skill for all the experiments performed (Figure 27). For salinity, the comparison with ARGO observations shows similar results for all the experiments, even if a higher RMSE, corresponding to a negative BIAS, is evident for experiment V5 in the first 100 m of the water column (Figure 28).

The RMSE and the BIAS for temperature (°C) and salinity (PSU) averaged on the western sub-basin are shown in Figure 29 and Figure 30 respectively.

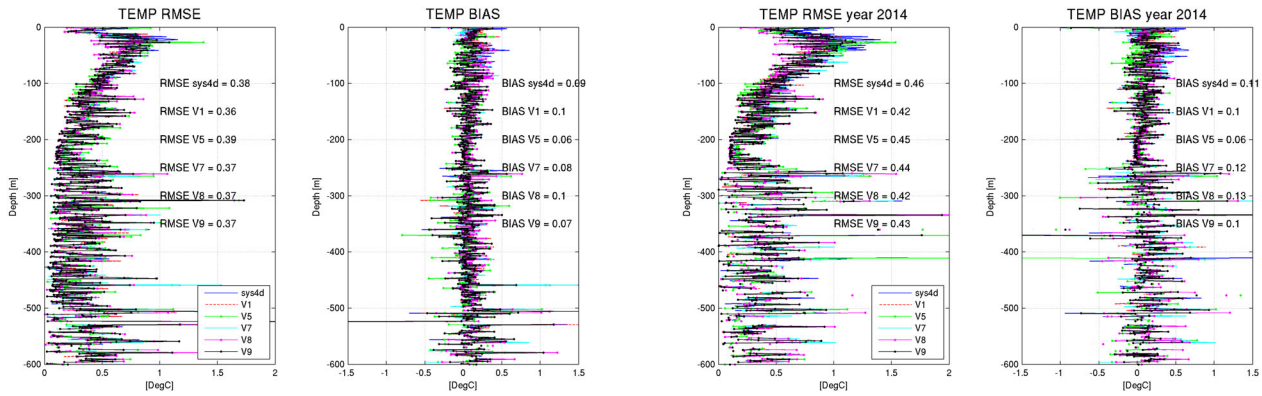

Figure 29. Root Mean Square Error (RMSE) and BIAS of temperature (°C) averaged on the western sub-basin for the whole simulation period (left-hand side panel) and for year 2014 only (right-hand side panel).

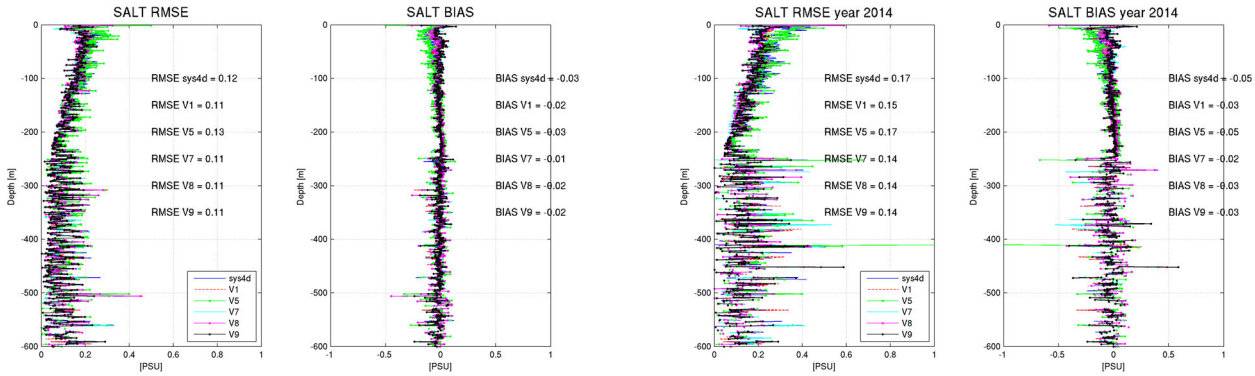

Figure 30. Root Mean Square Error (RMSE) and BIAS of salinity (PSU) averaged on the western sub-basin for the whole simulation period (left-hand side panel) and for year 2014 only (right-hand side panel).

In the western sub-basin all the experiments show similar results for temperature; V5 has the higher RMSE (Figure 29). For salinity for the entire basin, the experiment V5 has higher salinity RMSE in the first 100 m of the water column, corresponding to a negative BIAS (Figure 30).

The RMSE and the BIAS for temperature (°C) and salinity (PSU) averaged on the central sub-basin are shown in Figure 31 and Figure 32 respectively.

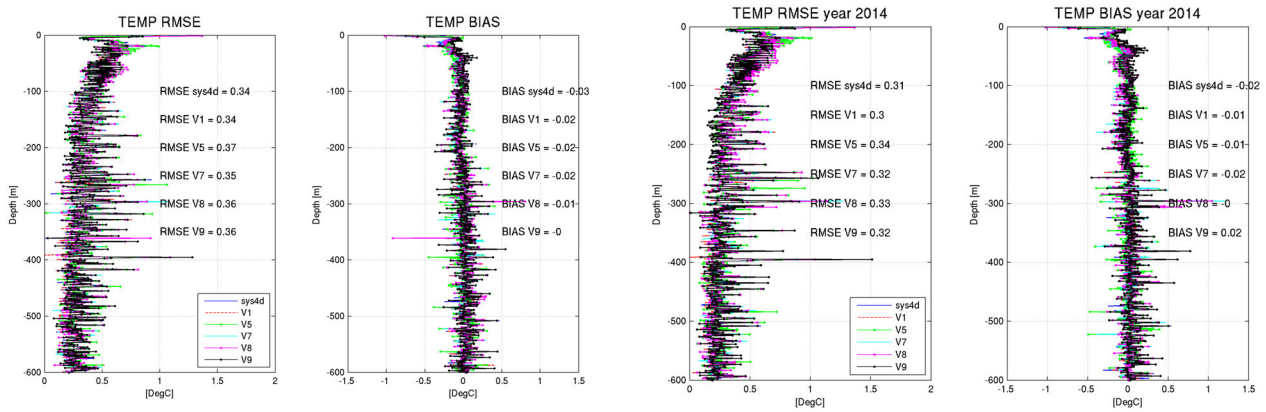

Figure 31. Root Mean Square Error (RMSE) and BIAS of temperature (°C) averaged on the central sub-basin for the whole simulation period (left-hand side panel) and for year 2014 only (right-hand side panel).

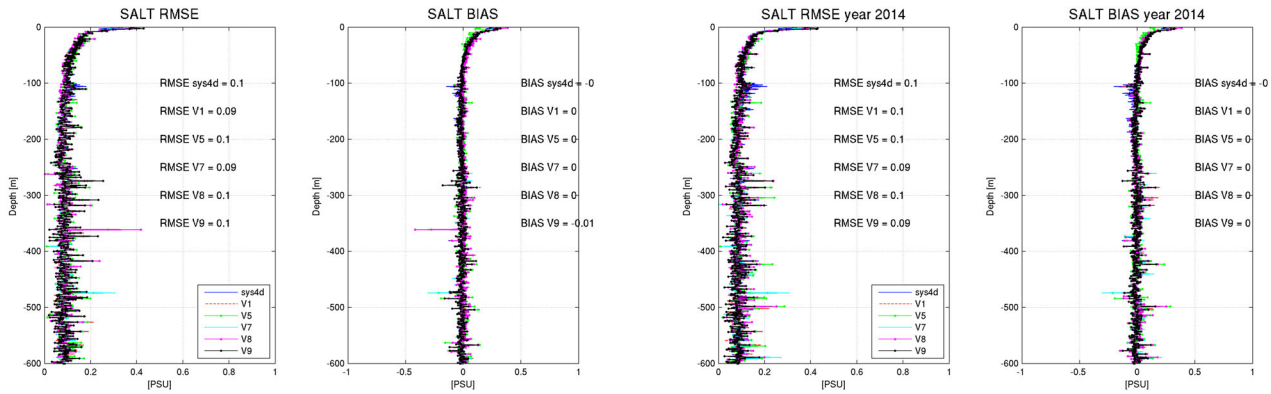

Figure 32. Root Mean Square Error (RMSE) and BIAS of salinity(PSU) averaged on the central sub-basin for the whole simulation period (left-hand side panel) and for year 2014 only (right-hand side panel).

In the central sub-basin the temperature (Figure 31) and salinity (Figure 32) comparison of all the experimental results with ARGO observations shows similar results, even if the experiment V5 shows the higher temperature RMSE.

The RMSE and the BIAS for temperature (°C) and salinity (PSU) averaged on the eastern sub-basin are shown in Figure 33 and Figure 34 respectively.

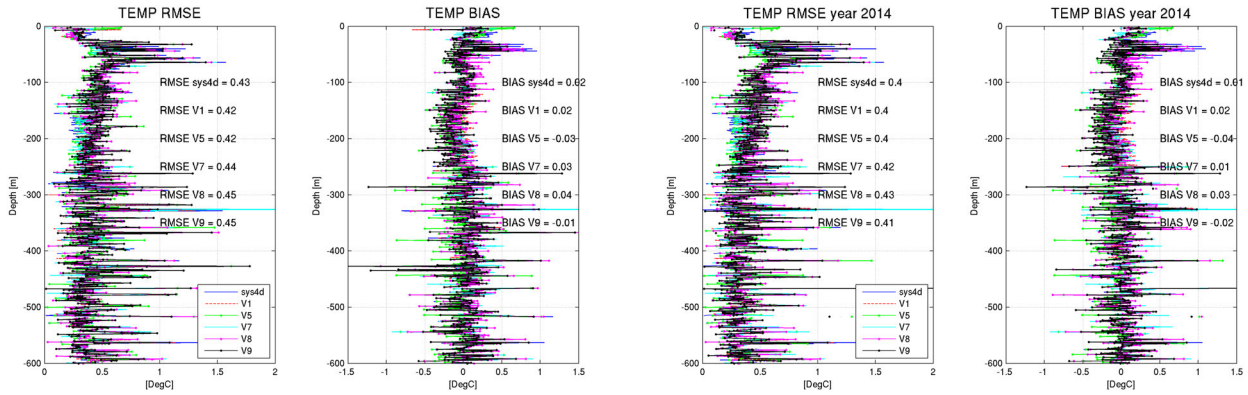

Figure 33. Root Mean Square Error (RMSE) and BIAS of temperature (°C) averaged on the eastern sub-basin for the whole simulation period (left-hand side panel) and for year 2014 only (right-hand side panel).

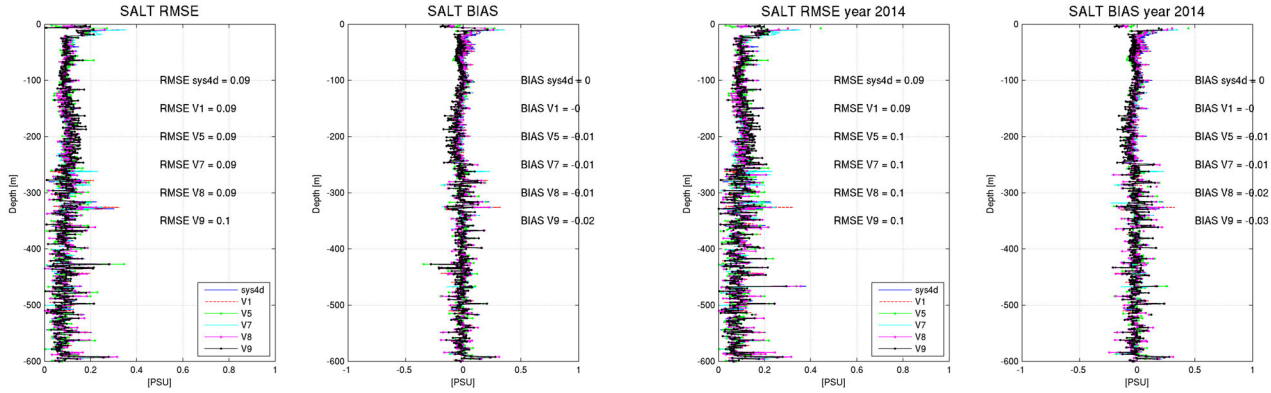

Figure 34. Root Mean Square Error (RMSE) and BIAS of salinity (PSU) averaged on the eastern sub-basin for the whole simulation period (left-hand side panel) and for year 2014 only (right-hand side panel).

The comparison of the experiments results for temperature with ARGO observations in the eastern basin shows the worst performances (Figure 33) among the three sub-basins considered. The comparison with ARGO salinity observations (Figure 34) shows a substantial agreement in the performances of all the experiments performed.

It can be noticed that computing BIAS and RMSE only for year 2014, and considering the year 2013 as spin-up time, the V9 experiment exhibit a clear skill improvement that is particularly evident considering temperature RMSE in the eastern sub-basin (Figure 33).

4.6 GLIDER Profiles (Temperature and Salinity) in the Balearic Sea

Comparing MFS sys4d outputs with data from glider observations in the Balearic Sea area it has been found that the model usually underestimates salinity and overestimates temperature at the sea surface.

The five experiments performed have been compared with MFS sys4d and with observations in order to evaluate the best model configuration in representing the vertical structure of salinity and temperature in the Balearic Sea area.

In the following three glider samples are shown, in order to highlight the differences between the model setups in the vertical salinity and temperature structure along the gliders tracks.

Figure 35 shows the comparison between model results and gliders observations for the period 6th February 2014 – 22nd February 2014, showing an improved temperature structure representation in experiment V9. In particular a cooling of the layer from surface up to 300 m depth is evident and in agreement with observations.

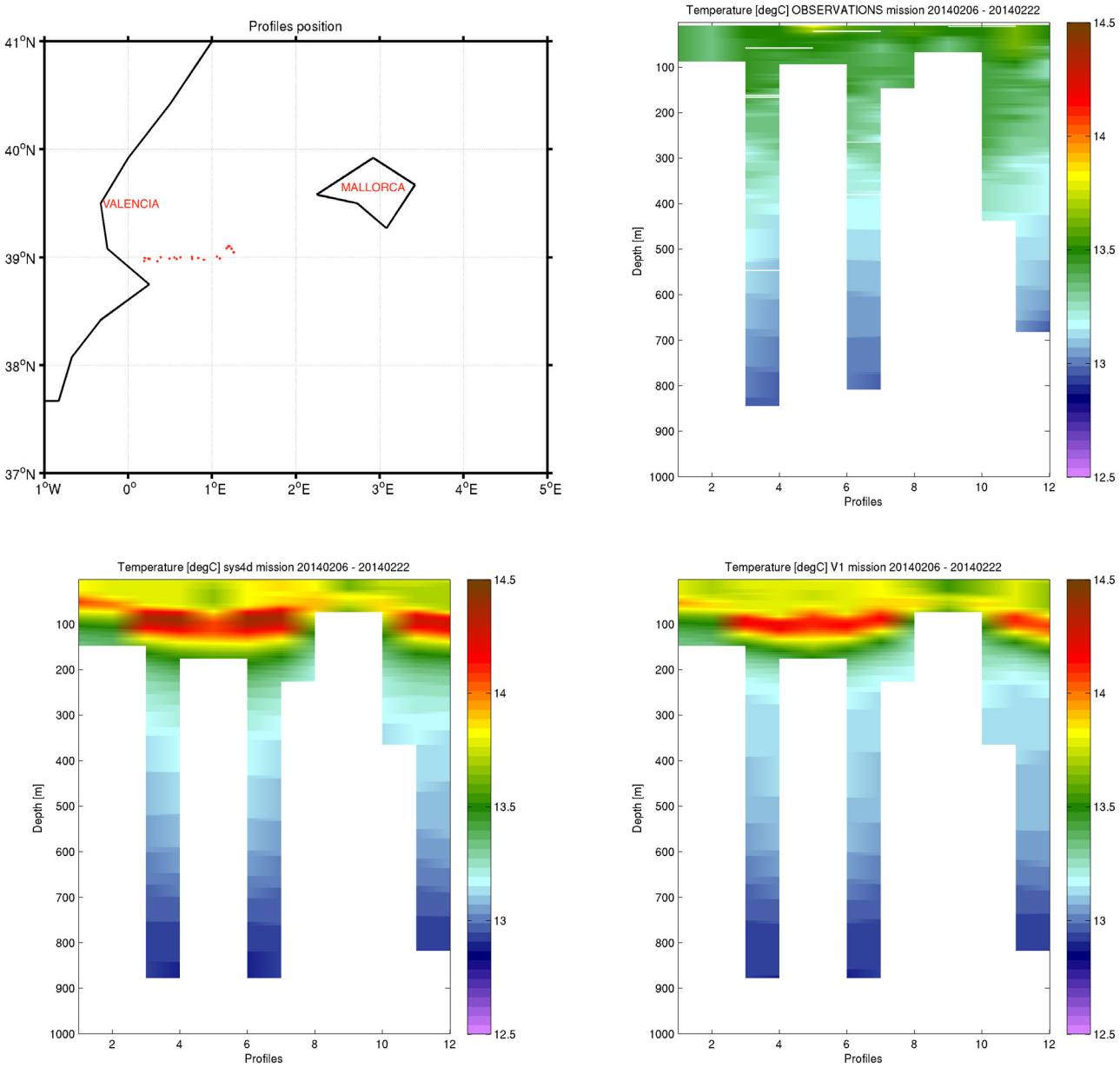

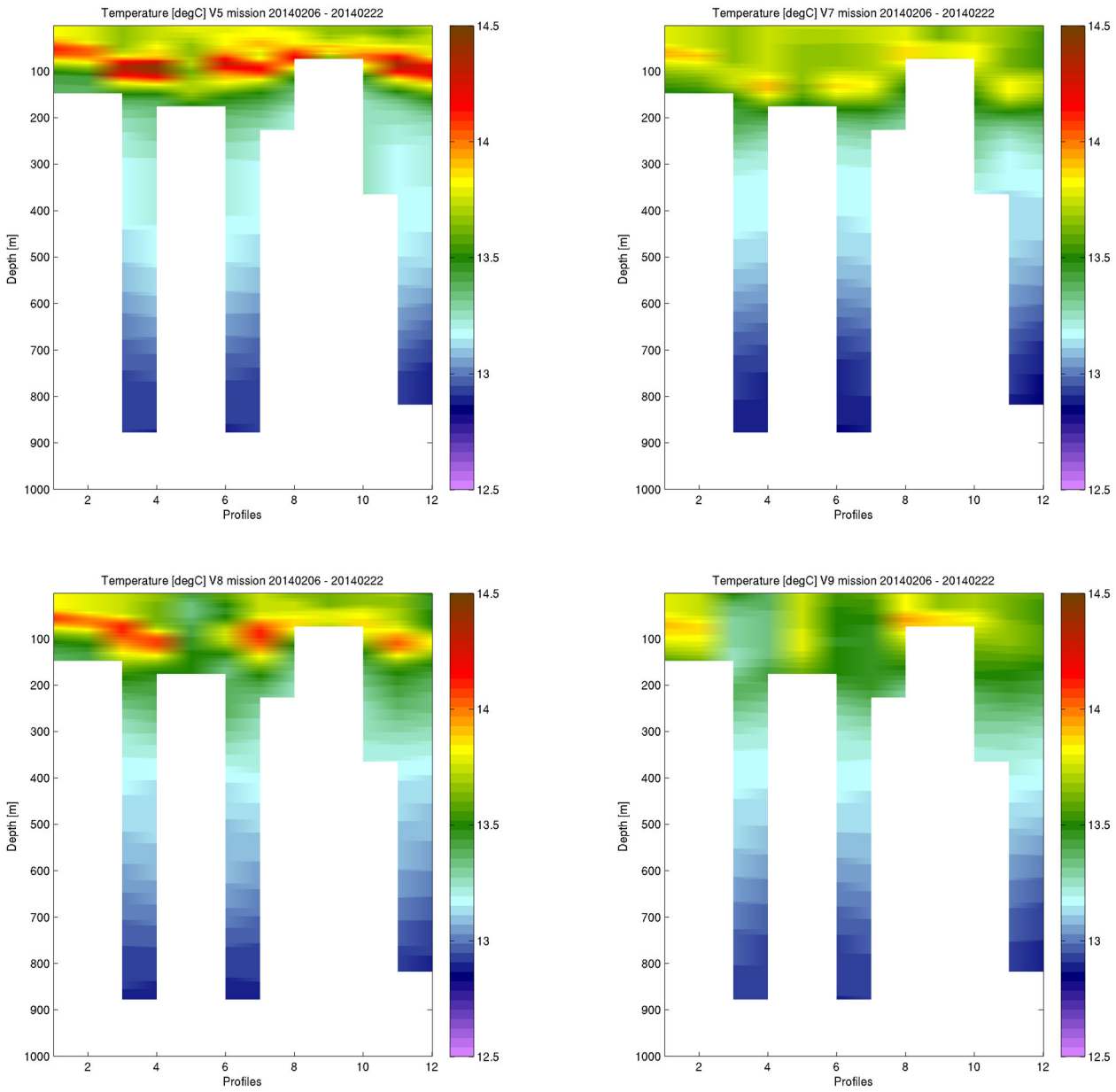

Figure 35. Comparison between temperature model results and gliders observations in the Balearic Sea area for the period: 6th February 2014 – 22nd February 2014.

In Figure 36 a comparison between salinity model results and gliders observations in the Balearic Sea area shows a good representation of salinity vertical structure in experiment V9. In particular the layer from surface up to 100 m depth is very well represented in experiment V9, with respect to the others experiments considered, and in evident agreement with observations.

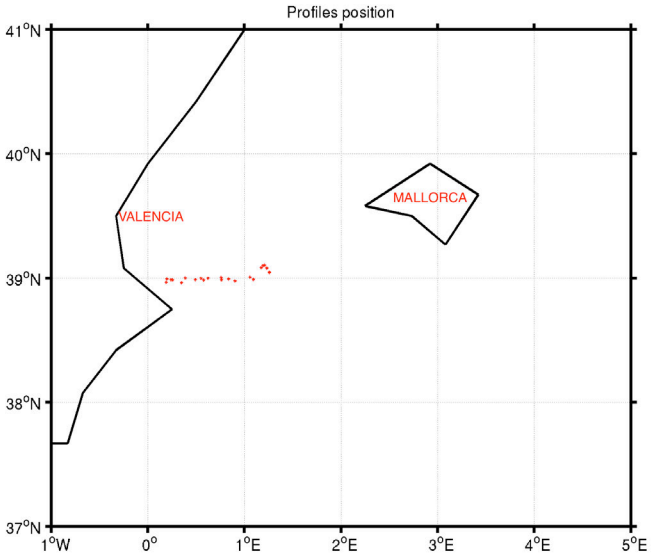
Profiles position
41°N
40°N
39°N
38°N
37°N
1°W
0°
1°E
2°E
3°E
4°E
5°E
VALENCIA
MALLORCA

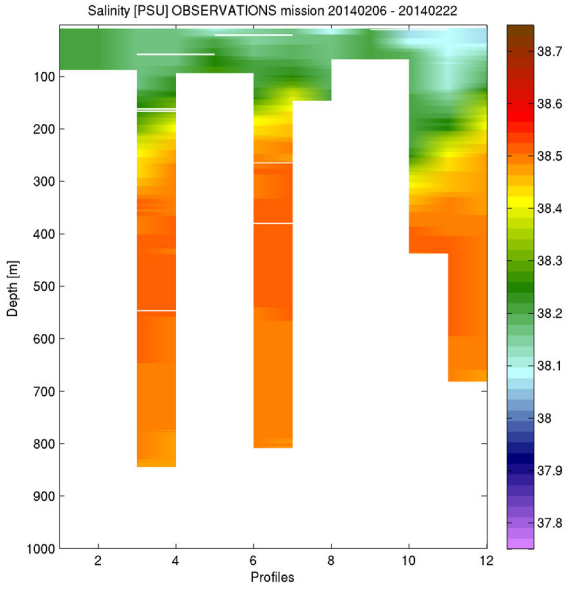
Salinity [PSU] OBSERVATIONS mission 20140206 - 20140222
Depth [m]
Profiles
38.7
38.6
38.5
38.4
38.3
38.2
38.1
38
37.9
37.8

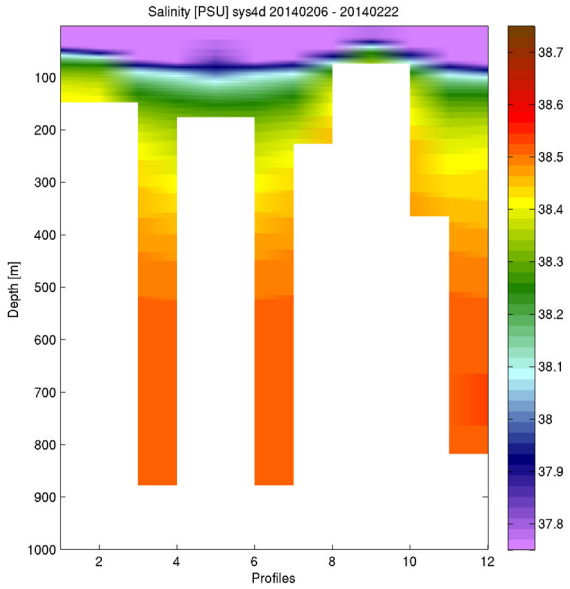
Salinity [PSU] sys4d 20140206 - 20140222
Depth [m]
Profiles
38.7
38.6
38.5
38.4
38.3
38.2
38.1
38
37.9
37.8

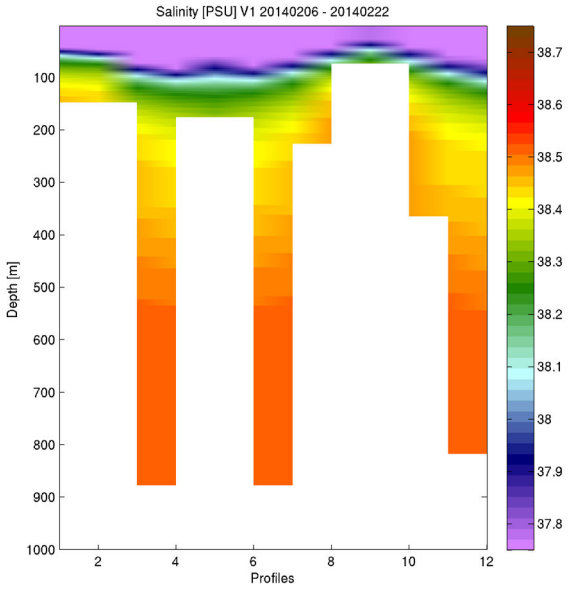
Salinity [PSU] V1 20140206 - 20140222
Depth [m]
Profiles
38.7
38.6
38.5
38.4
38.3
38.2
38.1
38
37.9
37.8

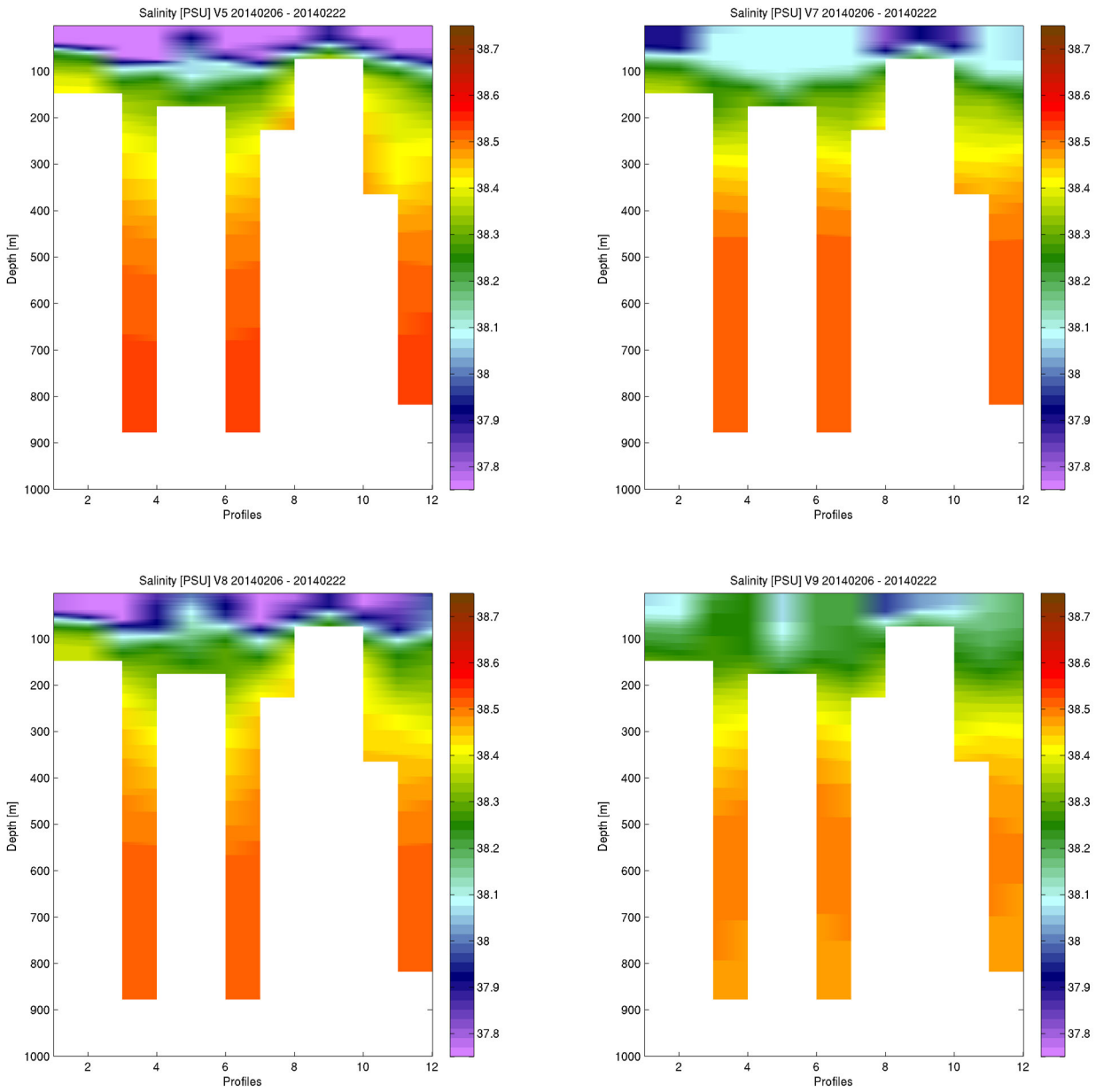

Figure 36. Comparison between salinity model results and gliders observations in the Balearic Sea area for the period: 6th February 2014 – 22nd February 2014.

Other salinity and temperature glider observations have been compared to the model results (not shown here for brevity). In some cases all the experiments results differ from the measurements and do not properly represent the surface layer up to 100 m depth. Usually experiment V9 provides a better representation of the tracers in the deep layer from 300 m depth to the bottom, as shown in Figure 37 for salinity for the period: 15th July 2013 – 29th July 2013.

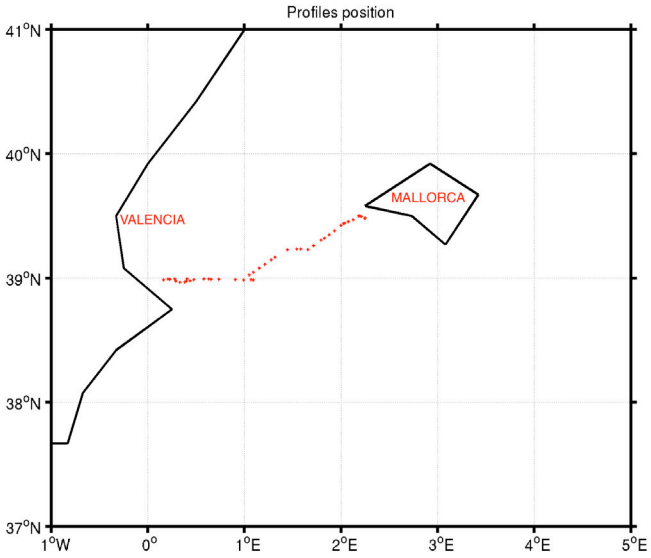
Profiles position
41°N
40°N
39°N
38°N
37°N
1°W
0°
1°E
2°E
3°E
4°E
5°E
VALENCIA
MALLORCA

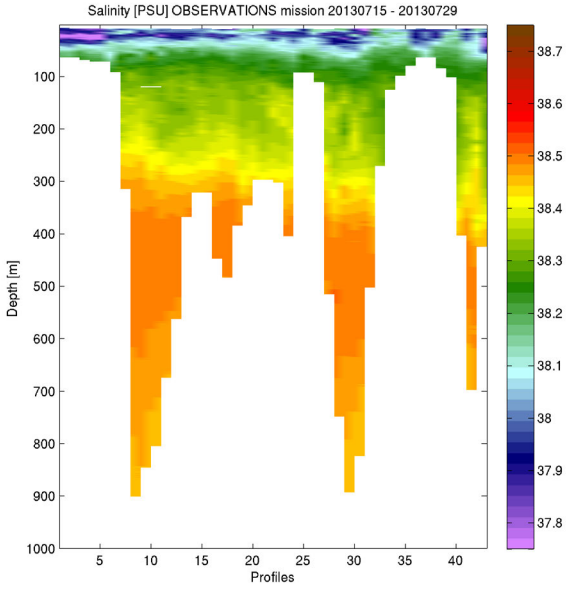
Salinity [PSU] OBSERVATIONS mission 20130715 - 20130729
Depth [m]
Profiles
38.7
38.6
38.5
38.4
38.3
38.2
38.1
38
37.9
37.8

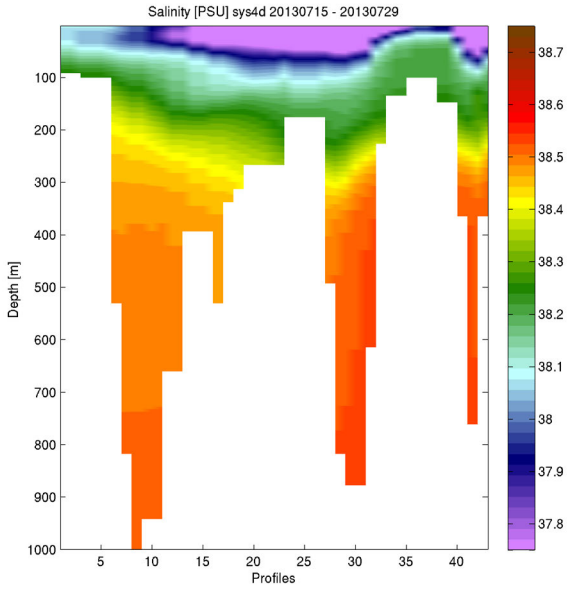
Salinity [PSU] sys4d 20130715 - 20130729
Depth [m]
Profiles
38.7
38.6
38.5
38.4
38.3
38.2
38.1
38
37.9
37.8

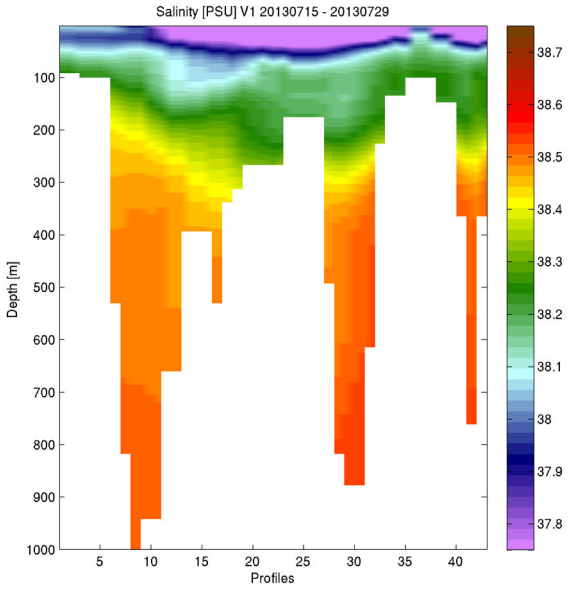
Salinity [PSU] V1 20130715 - 20130729
Depth [m]
Profiles
38.7
38.6
38.5
38.4
38.3
38.2
38.1
38
37.9
37.8

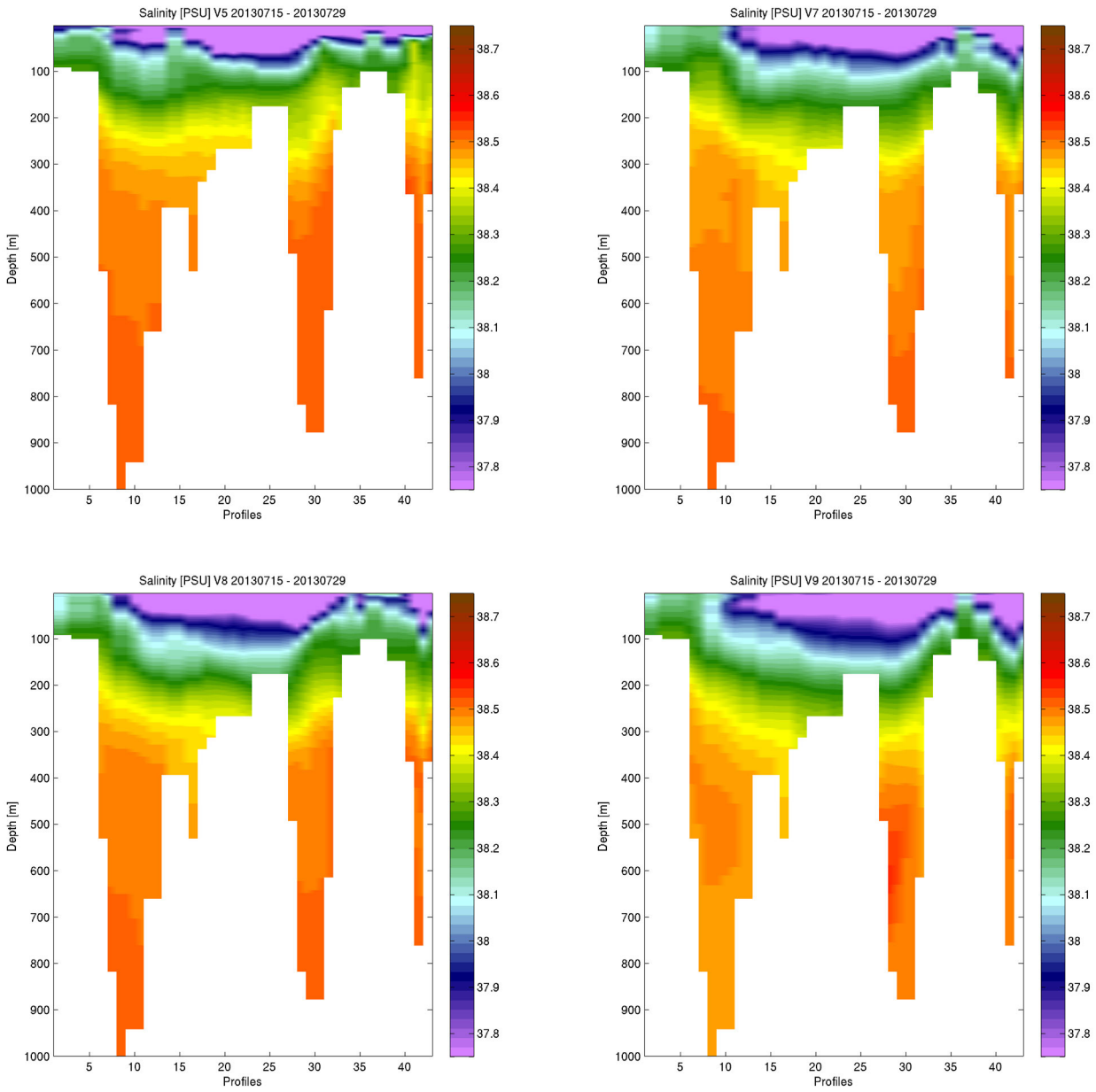

Figure 37. Comparison between salinity model results and gliders observations in the Balearic Sea area for the period 15th July 2013 – 29th July 2013.

4.7 T/S Diagrams in the Balearic Sea area

T/S diagrams for Balearic Sea area have been evaluated in order to understand the temperature/salinity distribution achieved by the numerical experiments performed and compare them with ARGO observations.

A comparison between all the experiments performed and the observations for the whole simulation period is shown in Figure 38.

JANUARY 2013 – SEPTEMBER 2014

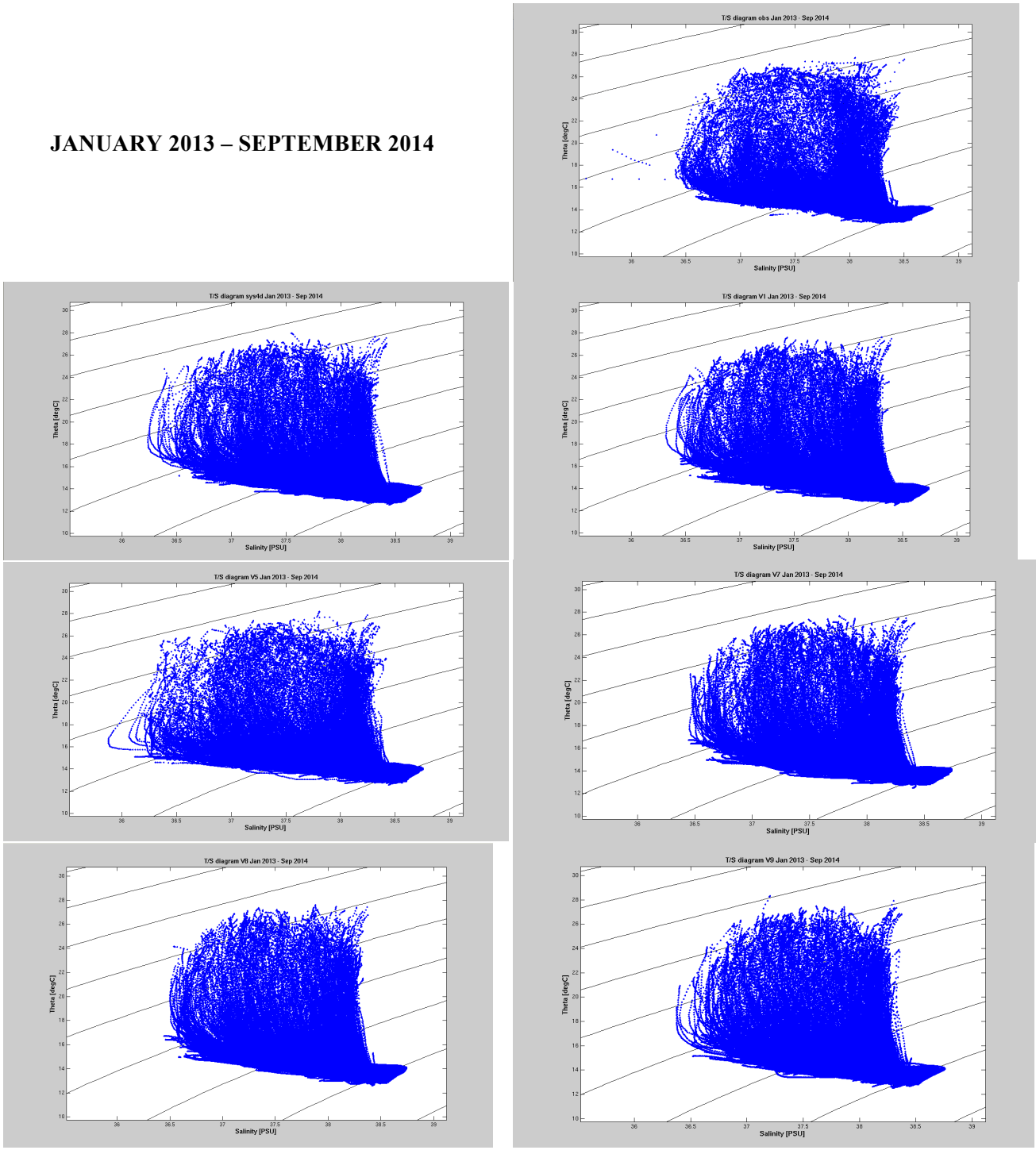

Figure 38. T/S diagram comparison for the whole simulation period (January 2013 – September 2014) in the Balearic Sea area.

The temperature/salinity distribution of the observations is well represented in experiments V7, V8 and V9, while in the other experiments the model salinity is lower than the observations, and temperature is higher than observations.

A comparison between all the experiments performed and observations for the sample period March – April 2014 is shown in Figure 39.

MARCH 2014 – APRIL 2014

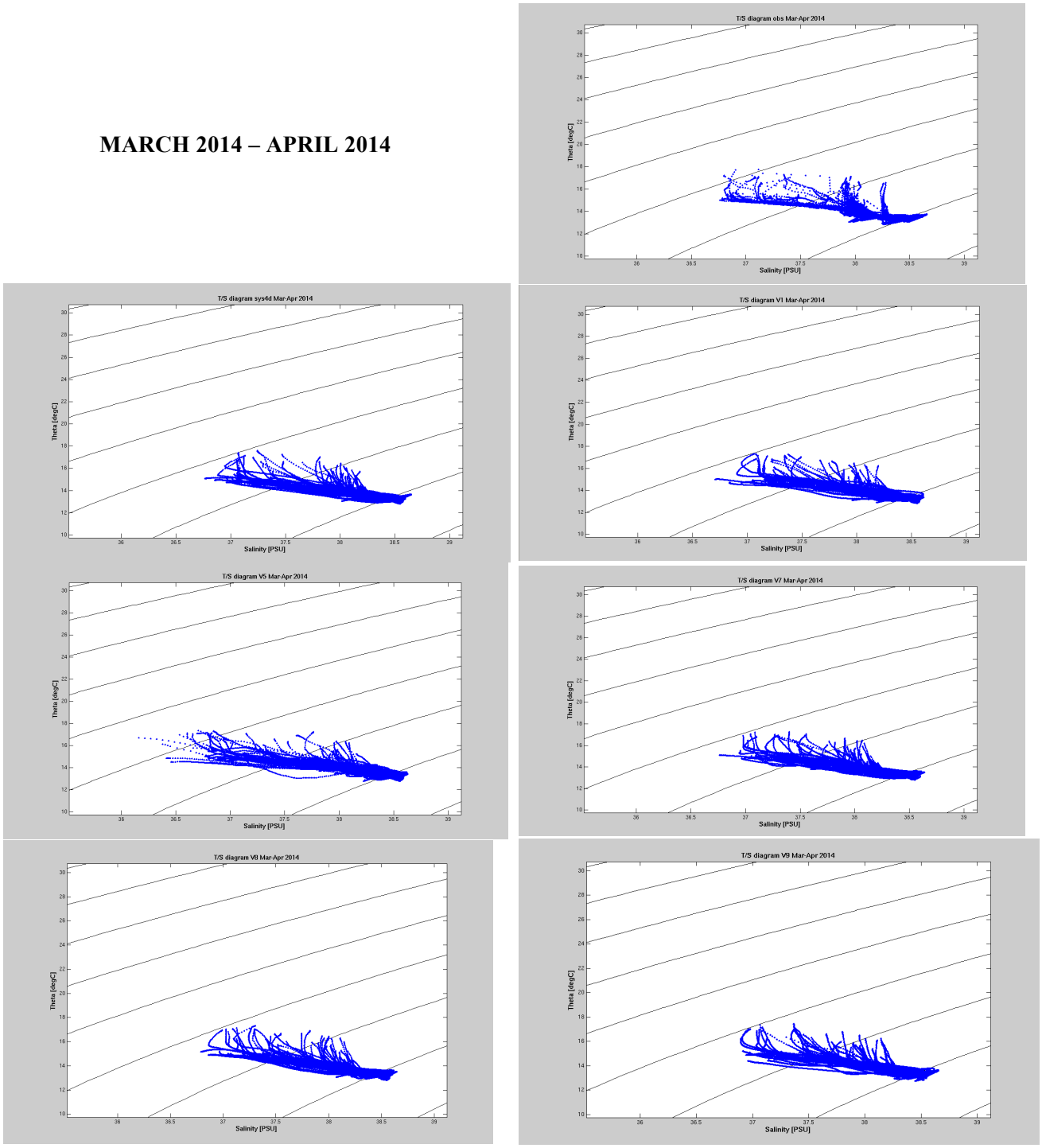

Figure 39. T/S diagram comparison for a sample spring simulation period (March 2014 – April 2014) in the Balearic Sea area.

Considering the summer period all the numerical experiments correctly reproduce the temperature/salinity distribution of observations, except V5 which shows a too low salinity with respect to the observations. In particular experiment V9 is in better agreement with the observations in reproducing the Levantine Intermediate Water (LIW) characteristics, the water masses close to the 37.5 isohaline in Figure 39.

4.8 Waves: basin averaged time series and CalVal buoys

Numerical wave model results are shown in terms of basin averaged time series of significant wave height (mean wave height of the highest third of the waves), mean wave period and peak wave period. Model results have been also validated by comparing wave height and periods to buoys measurements using the CalVal tool.

The basin averaged time series of the investigated parameters show similar results for all the experiments performed, and the differences between the experiments results and MFS sys4d run are shown in Figure 40, 41 and 42.

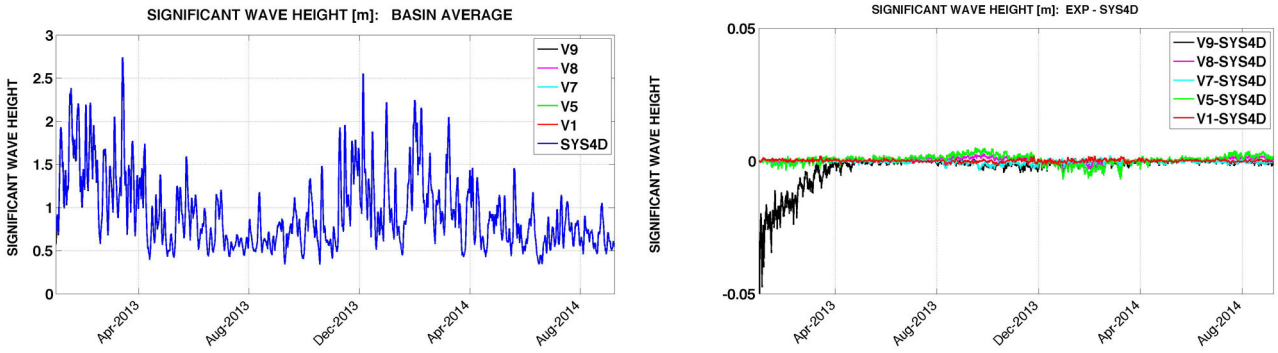

Figure 40. Basin averaged significant wave height comparison (left-hand side panel) and differences between the experiments performed and MFS sys4d run (right-hand side panel) for the whole period of simulation.

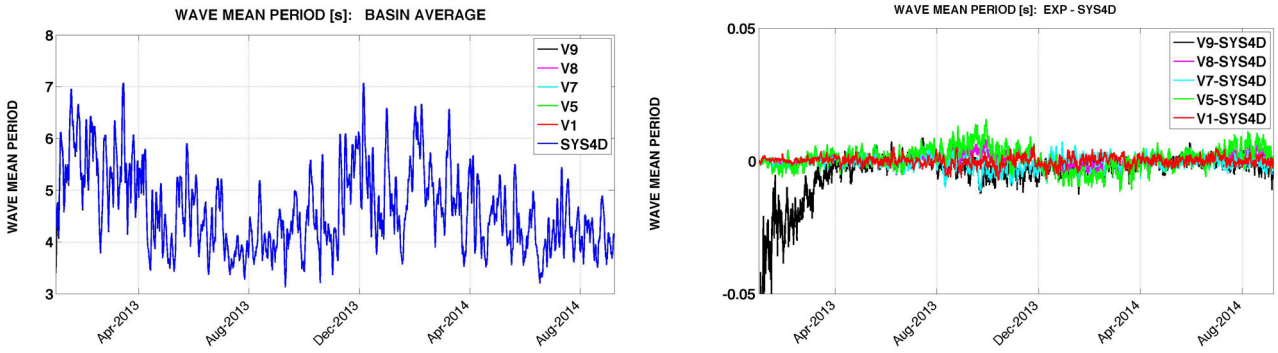

Figure 41. Basin averaged mean wave period comparison (left-hand side panel) and differences between the experiments performed and MFS sys4d run (right-hand side panel) for the whole period of simulation.

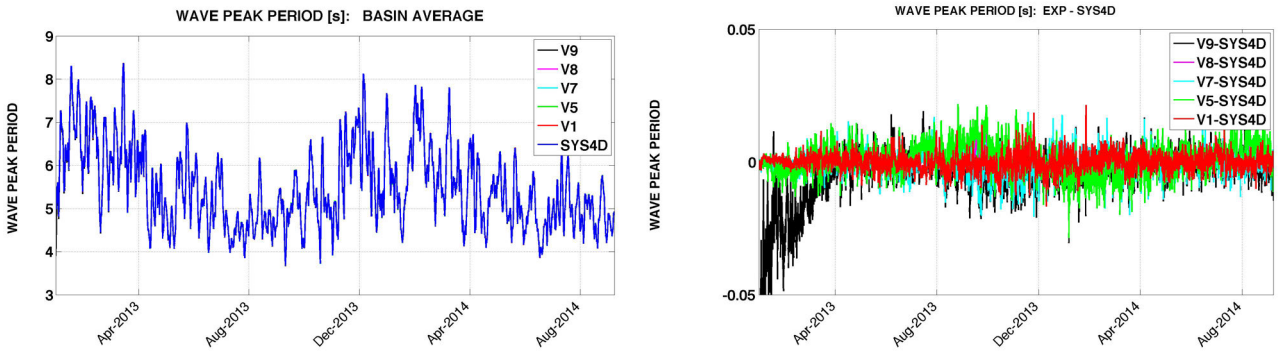

Figure 42. Basin averaged peak wave period comparison (left-hand side panel) and differences between the experiments performed and MFS sys4d run (right-hand side panel) for the whole period of simulation.

The intercomparison between the performed experiments show extremely small differences in terms of basin averaged significant wave height and periods.

Considering the differences between the performed experiments and the sys4d run, Figures 40 to 42 highlight that the largest differences occur in late summer – winter period, when the wave field has the highest variability.

Experiments V5 and V9 have the largest differences with respect to sys4d, in particular experiment V9 differences are mainly concentrated during the first 4 months of simulation due to the climatological initial conditions.

The comparison of model results with CalVal buoys shows that all the performed experiments produce very similar results.

The CalVal comparisons for Capo Mele station in terms of significant wave height, mean and peak periods are shown as an example in Figure 43.

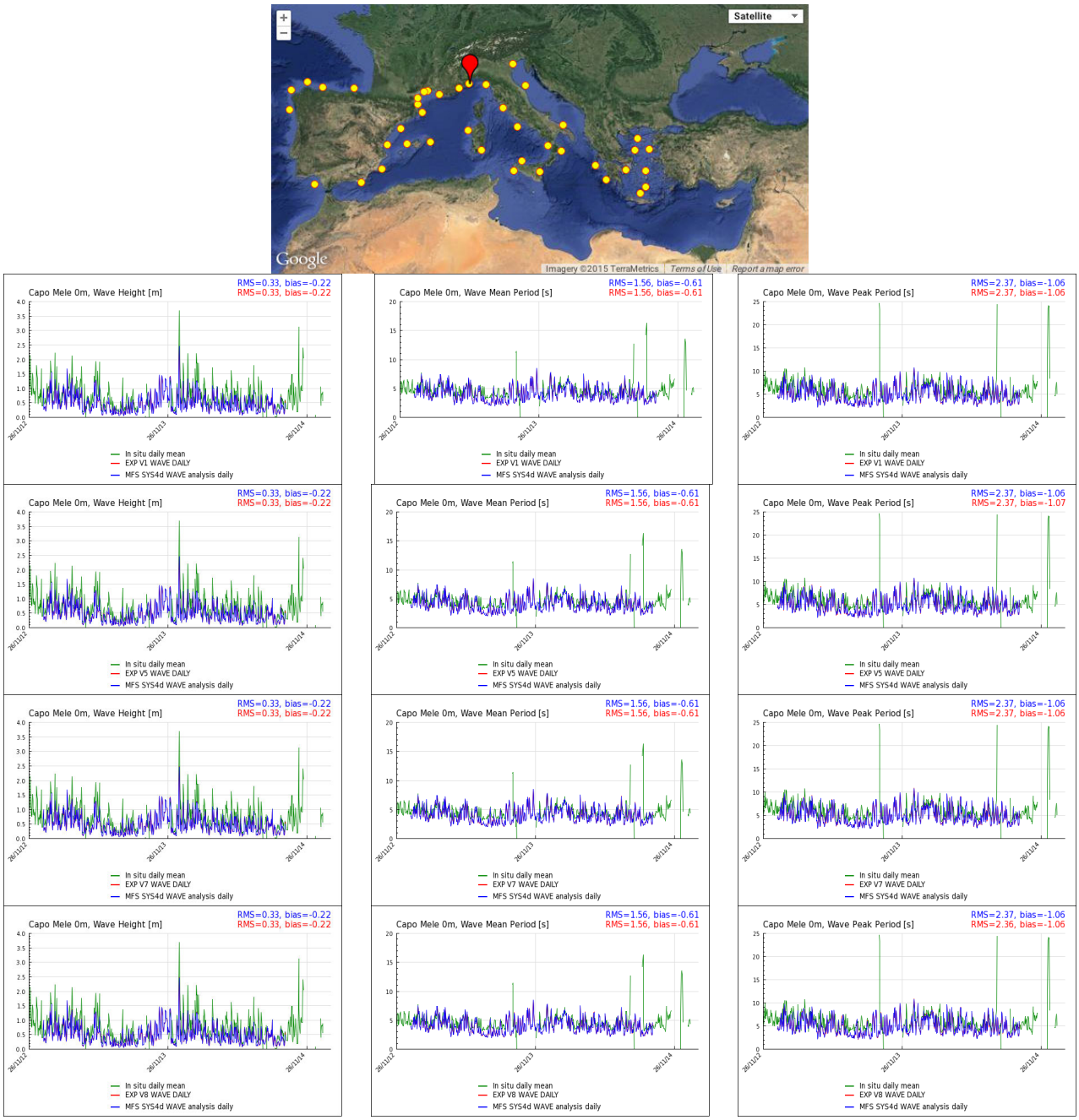

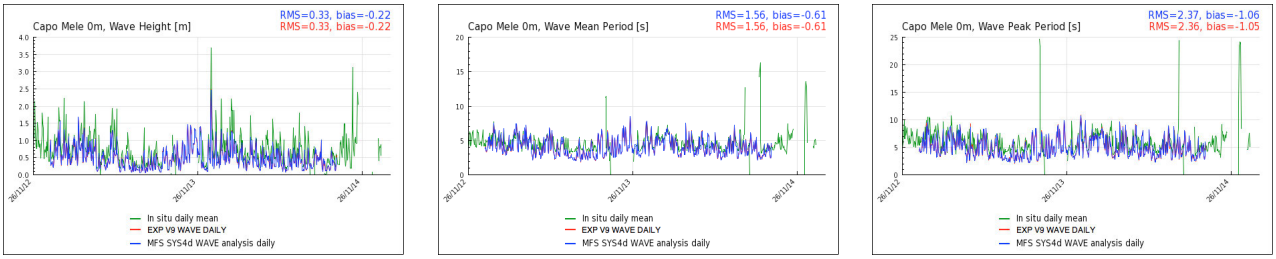

Figure 43. Root Mean Square Error of significant wave height, mean wave period and peak wave period of the performed experiments at Capo Mele station.

As shown in Figure 43, the wave model results are only slightly affected by the ocean circulation model modifications, remaining the main statistics (RMSE and bias) unchanged when considering all the numerical experiments carried out.

5. Conclusions

The validation of the numerical experiments performed against in situ and remote sensing measurements shows that experiment V7 has the best performances among the experiments considered, in terms of temperature, salinity, sea surface height and currents representation skill.

The experiment V9 confirms the improvements of V7 experiment skills when initialized from temperature and salinity climatologies instead of from a restart of sys4d operational system.

Indeed, considering the year 2013 as spin-up time, the Estimated accuracy numbers analysis for 2014 shows that the V9 experiment has the best performances for volume salinity, sea level anomaly and sea surface temperature, while for volume temperature the results are similar to the V7 ones (Figure 24 and Table 10).

The V7 and V9 experiments lead to a better representation of the tracers in the deep layer from 300 m depth to the bottom in Balearic Sea area, and in some cases a big improvement in surface and subsurface salinity and temperature representation can be noticed.

The different setups tested in the performed experiments seem not to have any significant impact on mean wave period, peak wave period and significant wave height computed by WWIII model.

In view of the results of the performed experiments it has been decided to use the setup of the V7 experiment in order to build the Mediterranean Forecasting System for MyOcean V5.

Moreover it has been decided to re-initialise the Mediterranean Forecasting System from SeaDataNet initial conditions, decision supported by the good results of experiment V9.

References

Clementi E., Oddo P., Korres G., Drudi M. and Pinardi, N., (2013). *Coupled wave-ocean modelling system in the Mediterranean Sea*. Extended abstract to the 13th Int. Workshop on Wave Hindcasting, Banff, Canada, 2013, 8 pp.

Dobricic S., (2005). *New mean dynamic topography of the Mediterranean calculated from assimilation system diagnostics*. Geophys. Res. Lett., 32, L11606, doi:10.1029/2005GL022518.

Dobricic S., Pinardi N., Adani M., Tonani M., Fratianni C., Bonazzi A. and Fernandez V., (2007). *Daily oceanographic analyses by Mediterranean Forecasting System at the basin scale*. Ocean Sci., 3, 149-157, 2007.

Dobricic S. and Pinardi N., (2008). *An oceanographic three-dimensional variational data assimilation scheme*. Ocean modelling, 22: 89-105 (2008), doi:10.1016/j.ocemod.2008.01.004.

Drevillon M., Bourdalle-Badie R., Derval C., Drillet Y., Lelouche J.M., Remy E., Tranchant B., Benkiran M., Greiner E., Guinehut S., Verbrugge N., Garric G., Testut C.E., Laborie M., Nouel L., Bahurel P., Bricaud C., Crosnier L., Dombrosky E., Durand E., Ferry N., Hernandez F., Le Galloudec O., Messal

F. and Parent L., (2008). *The GODAE/MercatorOcean global ocean forecasting system: results, applications and prospects*. J. Operational Oceanogr., 1(1), 51–57, 2008.

Fekete B.M., Vorosmarty C.J. and Grabs W., (1999). *Global, Composite Runoff Fields Based on Observed River Discharge and Simulated Water Balances*. Tech. Rep. 22, Global Runoff Data Cent., Koblenz, Germany, 1999.

Flather R.A., (1976). *A tidal model of the northwest European continental shelf*. Memories de la Societe Royale des Sciences de Liege 6 (10), 141–164.

Gunther H., Hasselmann H. and Janssen P.A.E.M., (1993). *The WAM model cycle 4*. DKRZ report n. 4, 1993.

Hasselmann K., (1974). *On the characterization of ocean waves due to white capping.* Boundary-Layer Meteorology, 6, 107-127.

Hasselmann S. and Hasselmann K, (1985). Computations and parameterizations of the nonlinear energy transfer in a gravity wave spectrum. Part I: *A new method for efficient computations of the exact nonlinear transfer integral*. J. Phys. Ocean., 15, 1369-1377.

Hasselmann S., Hasselmann K, Allender J.H. and Barnett T.P., (1985). *Computations and parameterizations of the nonlinear energy transfer in a gravity wave spectrum. Part II: Parameterizations of the nonlinear energy transfer for application in wave models*. J. Phys. Ocean., 15, 1378-1391, 1985.

Janssen P.A.E.M., (1989). *Wave induced stress and the drag of air flow over sea wave.* J. Phys. Ocean., 19, 745-754.

Janssen P.A.E.M., (1991). *Quasi-Linear theory of wind wave generation applied to wave forecasting*. J. Phys. Ocean., 21, 1631-1642.

Komen G.J., Hasselmann S. and Hasselmann K., (1984). *On the existence of a fully developed windsea spectrum*. J. Phys. Ocean., 14, 1271-1285.

Kourafalou V.H. and Barbopoulos K., (2003). *High resolution simulations on the North Aegean Sea seasonal circulation*. Ann. Geophys., 21, 251–265, 2003 - http://www.ann-geophys.net/21/251/2003/.

Levy M., Estubier A. and Madec G., (2001). *Choice of an advection scheme for biogeochemical ocean models.* Geophys. Res. Lets, 28, 19, 3725-3728.

Madec G., (2008). *NEMO ocean engine*. France, Institut Pierre-Simon Laplace (IPSL), 300pp. (Note du Pole de Modélisation 27).

Marchesiello P., McWilliams J.C. and Shchepetkin A., (2001). *Open boundary conditions for long-term integration of regional oceanic models*. Ocean Modelling, 3, 1-20.

Noh Y. (2004). *Sensitivity to wave breaking and the Prandtl number in the ocean mixed layer model and its dependence on latitude.* Geophys. Res. Let t., 31, L 23305, doi:10.1029/2004GL021289.

Oddo P., Adani M., Pinardi N., Fratianni C., Tonani M., Pettenuzzo D., (2009). *A Nested Atlantic-Mediterranean Sea General Circulation Model for Operational Forecasting*. Ocean Sci., 5, 461-473, doi:10.5194/os-5-461-2009, 2009.

Oddo P., Bonaduce A., Pinardi N. and Guarnieri A., (2014). *Sensitivity of the Mediterranean sea level to atmospheric pressure and free surface elevation numerical formulation in NEMO*. Geosci. Model Dev., 7, 3001–3015, 2014.

Pinardi N., Allen I., De Mey P., Korres G., Lascaratos A., Le Traon P.Y., Maillard C., Manzella G. and Tziavos C., (2003). *The Mediterranean ocean Forecasting System: first phase of implementation (1998-2001)*. Ann. Geophys., 21, 1, 3-20.

Raicich F., (1996). *On fresh water balance of the Adriatic Sea*. J. Mar. Syst., 9, 305–319.

Roullet G. and Madec G., (2000). *Salt conservation, free surface, and varying levels : a new formulation for ocean general circulation models*. J. Geophys. Res, 105, 23, 927–23, 942.

Tolman H.L., (2002). *Validation of WAVEWATCH III version 1.15 for a global domain*. NOAA / NWS / NCEP / OMB Technical Note 213, 33 pp.

Tolman H.L., (2009). *User manual and system documentation of WAVEWATCH III version 3.14*. 194 pp.

Tonani M., Pinardi N., Dobricic S., Pujol I. and Fratianni C., (2008). *A high-resolution free-surface model of the Mediterranean Sea*. Ocean Sci., 4, 1–14, http://www.ocean-sci.net/4/1/2008/.

Xie P. and Arkin P.A., (1997). *Global precipitation: A 17-year monthly analysis based on gauge observations, satellite estimates, and numerical model outputs*. B. Am. Meteorol. Soc., 78, 2539–2558.

ISSN 1590-2595

Quaderni di Geofisica

http://istituto.ingv.it/l-ingv/produzione-scientifica/quaderni-di-geofisica/

I Quaderni di Geofisica coprono tutti i campi disciplinari sviluppati all'interno dell'INGV, dando particolare risalto alla pubblicazione di dati, misure, osservazioni e loro elaborazioni anche preliminari, che per tipologia e dettaglio necessitano di una rapida diffusione nella comunità scientifica nazionale ed internazionale. La pubblicazione on-line fornisce accesso immediato a tutti i possibili utenti. L'Editorial Board multidisciplinare garantisce i requisiti di qualità per la pubblicazione dei contributi.

ISSN 2039-7941

rapporti tecnici INGV

http://istituto.ingv.it/l-ingv/produzione-scientifica/rapporti-tecnici-ingv/

I Rapporti Tecnici INGV pubblicano contributi, sia in italiano che in inglese, di tipo tecnologico e di rilevante interesse tecnico-scientifico per gli ambiti disciplinari propri dell'INGV. La collana Rapporti Tecnici INGV pubblica esclusivamente on-line per garantire agli autori rapidità di diffusione e agli utenti accesso immediato ai dati pubblicati. L'Editorial Board multidisciplinare garantisce i requisiti di qualità per la pubblicazione dei contributi.

ISSN 2039-6651

Miscellanea INGV

http://istituto.ingv.it/l-ingv/produzione-scientifica/miscellanea-ingv/

La collana Miscellanea INGV nasce con l'intento di favorire la pubblicazione di contributi scientifici riguardanti le attività svolte dall'INGV (sismologia, vulcanologia, geologia, geomagnetismo, geochimica, aeronomia e innovazione tecnologica). In particolare, la collana Miscellanea INGV raccoglie reports di progetti scientifici, proceedings di convegni, manuali, monografie di rilevante interesse, raccolte di articoli ecc..

Coordinamento editoriale e impaginazione
Centro Editoriale Nazionale | INGV

Progetto grafico e redazionale
Daniela Riposati | Laboratorio Grafica e Immagini | INGV

Via di Vigna Murata, 605
00143 Roma
Tel. +39 06518601 Fax +39 065041181

http://www.ingv.it

Istituto Nazionale di Geofisica e Vulcanologia